iScience

CellPress
OPEN ACCESS

Article

Lipids from a snail host regulate the multicellular behavior of a predator of parasitic schistosomes

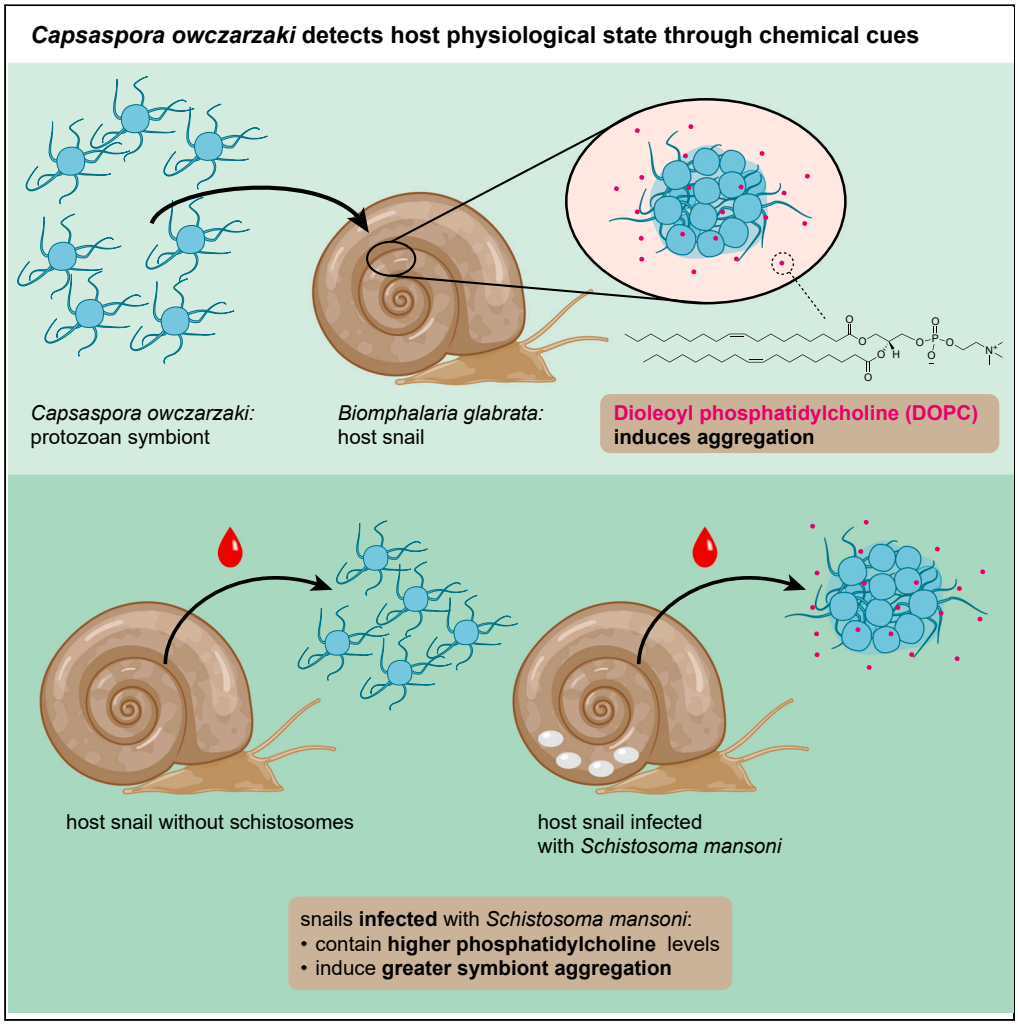

Ria Q. Kidner, Eleanor B. Goldstone, Martina R. Laidemitt, ..., Jamie Morris, W. Sean Davidson, Joseph P. Gerdt

jpgerdt@iu.edu

Highlights

Capsaspora forms multicellular aggregates within host snail tissue and snail serum

The snail serum phosphatidylcholine lipid DOPC induces *Capsaspora* aggregation

Schistosome-infected snails have more DOPC, causing greater *Capsaspora* aggregation

Chemically regulated aggregation may help *Capsaspora* survive its host environment

Kidner et al., iScience 27, 110724
September 20, 2024
https://doi.org/10.1016/j.isci.2024.110724

iScience

CellPress
OPEN ACCESS

Article

Lipids from a snail host regulate the multicellular behavior of a predator of parasitic schistosomes

Ria Q. Kidner,[1] Eleanor B. Goldstone,[1] Martina R. Laidemitt,[2] Melissa C. Sanchez,[2] Catherine Gerdt,[1] Lorin P. Brokaw,[1] Núria Ros-Rocher,[3] Jamie Morris,[4] W. Sean Davidson,[4] and Joseph P. Gerdt[1,5,*]

SUMMARY

Transmission of vector-borne diseases can be slowed by symbionts within the secondary hosts that spread disease. Snails spread schistosomiasis, and the snail symbiont *Capsaspora owczarzaki* kills schistosome larvae. In studying how *Capsaspora* colonizes its host snail, we discovered that *Capsaspora* responded to its host by forming multicellular aggregates. We elucidated the chemical cue for aggregation: hemolymph phosphatidylcholines (PCs). Furthermore, we uncovered that *Capsaspora* cells aggregate to different degrees in sera from different host snails—and these responses correlate with serum concentrations of PCs. Therefore, *Capsaspora* senses a host factor that can indicate the identity and physiological state of its host. Since cellular aggregation controls microbial motility, feeding, and immune evasion, this response within host tissue may be important for colonization. If so, snail serum PC and *Capsaspora* aggregation will be molecular and cellular markers to discern which conditions will favor the colonization of snails (and potential exclusion of schistosomes) by *Capsaspora*.

INTRODUCTION

Microbial symbionts frequently impact the fitness of their animal hosts—both for the better and the worse.[1,2] Due to their abundance and ease of study, bacterial symbionts have garnered the most research. However, microbial *eukaryotes* (i.e., protists) also frequently influence their hosts.[3] Although pathogens are the best studied eukaryotic symbionts (e.g., *Plasmodium*, *Leishmania*, *Candida*, and chytrids),[4–7] mutualist and commensal microeukaryotes also populate the literature.[8–10] The protist *Capsaspora owczarzaki* (hereafter "*Capsaspora*") is an intriguing symbiont of snails that may *both* reveal insight into protist-animal symbioses *and* curtail the spread of neglected tropical diseases.[11,12]

Capsaspora was initially isolated as unicellular filopodiated amebae from the pericardia and mantles of *Biomphalaria glabrata* (Figure 1A). This snail is also the intermediate host that transmits *Schistosoma mansoni*, the causative agent of intestinal human schistosomiasis in Africa and the Neotropics.[11,12] Due to its disease relevance, *Biomphalaria* snails have been well studied in the laboratory for decades.[13–17] More recently, *Capsaspora* has also become an emerging experimental model with substantial "omic" resources[18–23] and molecular tools available,[24–27] making this snail-amoeba symbiosis ideally suited for deeper analysis as a model system. More significantly, *Capsaspora* can readily adhere to and kill schistosomes while they are sporocysts (the intramolluscan growth stage) *in vitro*.[12,28] Therefore, *Capsaspora* may be able to halt the spread of schistosomiasis by outcompeting schistosomes within their intermediate host snails—similar to how *Wolbachia* bacteria halt the spread of mosquito-transmitted diseases.[29–31] Since the ~300 million people who suffer snail-transmitted diseases can be difficult to treat, such an ecological intervention to deplete parasites in endemic areas is an attractive approach.[32–34] However, the interactions between *Capsaspora*, *Biomphalaria* snails, and schistosome parasites are still poorly understood.[11,12,28,35]

Although *Capsaspora* has been isolated from multiple inbred lines of *B. glabrata*[11] and molecularly detected by sequencing from wild snails,[36] it remains absent from many *B. glabrata* snails in the laboratory and the wild. Moreover, it is unknown which host factors determine *Capsaspora*'s ability to colonize the snail, and it is also unclear what fitness impact *Capsaspora* has on its host snail and co-resident parasites. Additionally, multiple life stages of *Capsaspora* have been described in the laboratory,[23] but it is unclear which life stages are relevant to its behavior inside the host snail (Figure 1B). In this study, we aimed to determine if *Capsaspora* could respond to chemical or cellular factors in its host snail environment.

[1]Department of Chemistry, Indiana University, Bloomington, IN 47405, USA
[2]Department of Biology, Center for Evolutionary and Theoretical Immunology, Parasite Division, Museum of Southwestern Biology, University of New Mexico, Albuquerque, NM 87131, USA
[3]Department of Cell Biology and Infection and Department of Developmental and Stem Cell Biology, Institut Pasteur, Université Paris-Cité, CNRS UMR3691, 25-28 Rue du Docteur Roux, 75015 Paris, France
[4]Department of Pathology and Laboratory Medicine, University of Cincinnati, Cincinnati OH 45237, USA
[5]Lead contact
*Correspondence: jpgerdt@iu.edu
https://doi.org/10.1016/j.isci.2024.110724

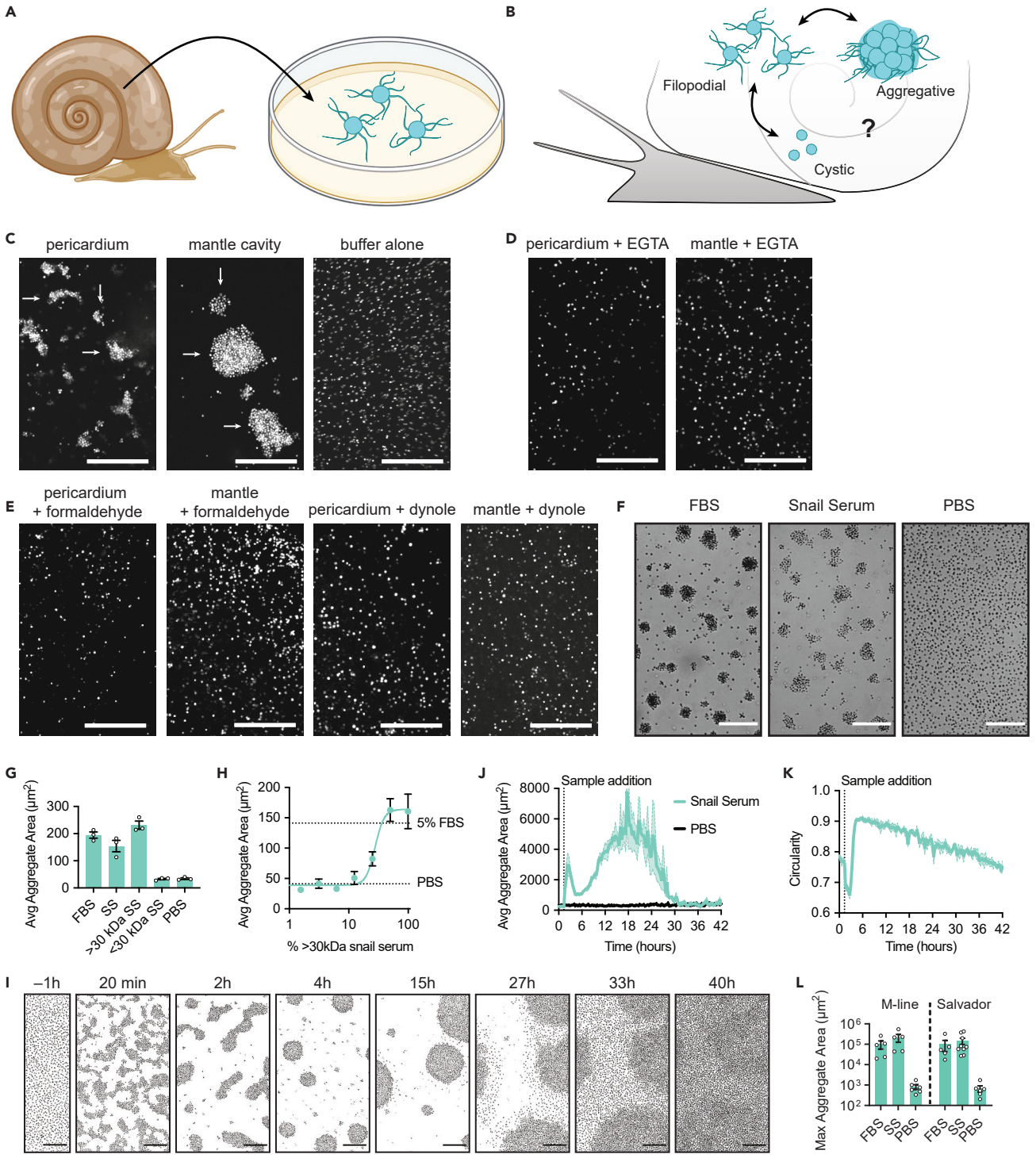

Figure 1. *Capsaspora* aggregates in response to snail tissue and serum

(A) *Capsaspora* was originally isolated from the pericardium and mantle of *B. glabrata*. Cells that grew out from snail samples were filopodiated.

(B) Known *Capsaspora* life stages: filopodiated amebae, cysts, and multicellular aggregates. It was previously unclear which life stages of *Capsaspora* are present inside snails.

(C) Representative images of tdTomato-expressing *Capsaspora* (ATCC 30864) aggregates observed after injection into *B. glabrata* (NMRI) snail tissues (left and center images) compared to a negative control where *Capsaspora* was injected directly onto a microscope slide with no snail (right image). Arrows indicate example aggregates. Scale bars are 100 μm.

Figure 1. *Continued*

(D) Representative images of *Capsaspora* co-injected with a calcium chelator (EGTA, 250 mM) into snail tissues—aggregation was prevented. Scale bars are 100 μm.

(E) Representative images of *Capsaspora* pre-treated for 30 min with and then co-injected with formaldehyde (4% [v/v]) or the endocytosis inhibitor dynole (20 μM) into snail tissues—aggregation was prevented. Scale bars are 100 μm.

(F) Representative images of *Capsaspora* aggregates induced by either 5% (v/v) FBS or 50% (v/v) snail serum in media compared to cells treated with 5% (v/v) phosphate-buffered saline (PBS) in media (negative control). Cells were imaged 90 min after addition of inducers. Scale bars are 100 μm.

(G) Average area of cell aggregates induced by FBS, snail serum (SS), and macromolecules (>30 kDa) and small molecules (<30 kDa) from snail serum.

(H) Dilution series of >30 kDa snail serum shows a dose-dependent induction of aggregation with an EC50 ~30% (v/v).

(I) Representative images showing cellular aggregates monitored for 2 days after addition of 50% (v/v) >30 kDa snail serum components. Images were converted to binary in FIJI to enhance contrast. Scale bar is 250 μm. The full time-lapse is available as Video S1.

(J) The average aggregate areas measured every 20 min for 42 h after addition of 50% (v/v) >30 kDa snail serum components.

(K) Average circularity of aggregates measured every 20 min for 42 h after addition of 50% (v/v) >30 kDa snail serum components shows initial snail serum-induced aggregates were elongated.

(L) Area of massive aggregates induced by either 10% (v/v) FBS or 50% (v/v) >30 kDa snail serum in two other isolated strains of *Capsaspora* (see images in Figure S5). All strains tested showed aggregation in response to snail serum. For plots, mean ± SEM (n = 3) are shown, and values from individual replicates are displayed with small circles.

We found that within snail host tissue, *Capsaspora* formed multicellular aggregates. These aggregates appeared similar to those formed by *Capsaspora* upon *in vitro* exposure to fetal bovine serum (FBS).[27] Furthermore, we discovered that the aggregation inducer in the snail serum is a specific phosphatidylcholine (PC) lipid (or possibly a suite of PC lipids). Remarkably, the concentration of this lipid in the snail hemolymph increased when the snail was infected with schistosomes, which led to significantly greater *Capsaspora* aggregation. *Capsaspora* also aggregated differently in hemolymph from different inbred snail lines. Therefore, *Capsaspora* can sense and respond to the physiological state and identity of its host snail. This work raises the hypothesis that a chemical mechanism of host discrimination may explain the presence of *Capsaspora* in some snails but not others. Further dissection of its *in vivo* aggregation and persistence may reveal the molecular requirements for *Capsaspora* to colonize its host and possibly exclude pathogenic schistosomes.

RESULTS

Capsaspora forms multicellular aggregates in snail tissue

Capsaspora behavior within its snail host has never been reported. To obtain an initial glimpse into the interaction of *Capsaspora* with its host snail, we introduced fluorescently labeled *Capsaspora* cells in their filopodial stage into naive *Biomphalaria glabrata* (NMRI, Naval Medical Research Institute) snails. The snails had no prior schistosome infection or colonization with *Capsaspora* (as evidenced by PCR, see Figures S1A and S1B). Since *Capsaspora* has been isolated from snail pericardial explants and mantle explants and swabs,[12] we injected *Capsaspora* cells into the pericardia and mantles. We discovered that *Capsaspora* formed multicellular aggregates within 5 min of injection into the tissue (Figure 1C, left and center images; Figures S1C and S1D). In contrast, *Capsaspora* imaged in the absence of snail tissue (in the injection buffer control) failed to aggregate (Figure 1C, right image), verifying that components of the snail triggered *Capsaspora* aggregation. Notably, these aggregates were reminiscent of the aggregates previously observed upon addition of FBS to *Capsaspora* cells *in vitro*.[27] Like FBS-induced aggregation, this aggregation phenotype was calcium dependent: co-injection of excess EGTA (ethylene glycol-bis(β-aminoethyl ether)-*N*,*N*,*N*′,*N*′-tetraacetic acid, a calcium-specific chelator) with *Capsaspora* into the snail pericardia and mantles suppressed the aggregation phenotype (Figure 1D). As seen previously with FBS, this aggregative phenotype required living *Capsaspora* cells[27] with active endocytic pathways.[37] Specifically, pre-treatment of *Capsaspora* with formaldehyde or an endocytosis inhibitor (dynole 34-2) prevented aggregation within snail tissue (Figure 1E). Therefore, cellular aggregation is likely an active response by living *Capsaspora* to the snail host. The observation of *Capsaspora* aggregation inside its natural snail host suggests that *Capsaspora*'s previously observed aggregation phenotype is ecologically relevant within the natural snail environment (not an artifact of artificial *in vitro* growth media).

Capsaspora forms multicellular aggregates in response to macromolecules in host snail serum

Capsaspora was also previously isolated from snail hemolymph.[11] Therefore, we asked whether hemolymph alone could induce *Capsaspora* aggregation *in vitro*. Indeed, sterile-filtered (0.22 μm) hemolymph from NMRI snails (hereafter "snail serum" or "SS") induced cellular aggregation (Figures 1F and 1G). Because the aggregate inducer previously found in FBS was a large lipoprotein complex,[27] we hypothesized that the inducer in snail serum was a macromolecule. To test this hypothesis, we fractionated snail serum using a 30 kDa molecular weight (MW) cutoff filter, and the large and small fractions were tested separately. As hypothesized, we found that >30 kDa snail serum induced robust aggregation, and the <30 kDa fraction did not (Figure 1G). Aggregation induced by >30 kDa snail serum was dose-dependent with an EC50 ~30% (v/v) (Figure 1H).

We monitored the kinetics of aggregate formation and dispersal in the presence of >30 kDa SS (Figure 1I; Video S1). Aggregates gradually formed over the course of several hours, peaked at ~18 h, and fully dispersed by 30 h (Figure 1J). The dispersal suggests a depletion of the aggregation-inducing substance. Aggregate morphology also changed over the course of the experiment. Initially elongated aggregates formed, and these coalesced into symmetric circular aggregates after 6 h (Figure 1K). Therefore, the chemical composition of the serum may change over time, influencing the specific morphology of the aggregates. Similar kinetics were observed when aggregation was induced

with >30 kDa FBS components. FBS-induced aggregates were also initially elongated, although the extent and duration of elongation depended on the exact dose (Figure S2; Video S1).

We also noticed that the snail serum-induced aggregates appeared less circular and less dense than those induced by FBS. This observation motivated us to characterize the aggregation morphology of *Capsaspora* cells induced by snail serum compared to FBS-induced aggregates via confocal microscopy. There were modest differences in aggregate sphericity, density, smoothness, and height (Figures S3A–S3D and S4). Interestingly, the morphological differences observed here under different chemical stimulation mirror some of the morphological differences reported in mutant *Capsaspora* strains.[26,38] Therefore, it is likely that multiple chemical and genetic factors contribute to the specific multicellular structures formed by *Capsaspora* cell-cell adhesion.

Finally, we determined if this aggregative behavior was conserved across multiple isolates of *Capsaspora* (or if it was possibly a phenotype unique to a single *Capsaspora* strain). In addition to the well-studied American Type Culture Collection (ATCC) 30864 *Capsaspora* strain,[22] we tested the ability of snail serum to induce aggregation of two other *Capsaspora* strains isolated separately from M-line and Salvador *B. glabrata* snails (ATCC 50973 and 50974, respectively).[11] The other two cultures are less studied and grow slower *in vitro*, possibly indicating less adaptation to laboratory culture conditions. They also attach less to the bottom of culture dishes, remaining suspended in the media. The altered growth required us to adapt our aggregation assay to a larger volume that included gentle agitation to encourage cell-cell contacts by suspended cells (see STAR Methods). In the adjusted aggregation assay, both of the alternative *Capsaspora* strains formed especially large aggregates in response to snail serum, as well as FBS (Figures 1L and S5). Therefore, we believe that the aggregative response of *Capsaspora* to *Biomphalaria* serum components is likely a widespread and natural *Capsaspora* phenotype. The original ATCC 30864 strain was used for further studies in this manuscript.

Together, these results suggest that serum-induced cellular aggregation is a relevant response of *Capsaspora* to its host snail environment. Furthermore, the aggregation inducer(s) are likely to be host-derived macromolecule(s) that are depleted over time by *Capsaspora*. We next sought to determine the specific identity of the aggregation inducer(s).

Lipids extracted from snail serum are sufficient to trigger aggregation

Low density lipoproteins (LDLs) were previously found to be the aggregation inducers in FBS.[27] Although snails do not have these lipoproteins,[39] we hypothesized that the macromolecular aggregation inducer(s) in snail serum were an analogous snail lipid complex. To test this hypothesis, we extracted the total lipids from snail serum and tested the solubilized lipid extract for aggregation induction. Indeed, we found that the crude lipids induced robust aggregation activity with an EC50 around 100 μg/mL (Figure 2A). This concentration was similar to the concentration of total lipids present in active dilutions of >30 kDa snail serum (see STAR Methods section), suggesting that lipids are sufficient to account for the aggregation induction activity in >30 kDa snail serum.

We then physically and chemically characterized these emulsified crude serum lipid particles that induced aggregation. First, we used transmission electron microscopy (TEM) to visualize particle sizes (Figure 2B) and dynamic light scattering (DLS) to determine the particle diameters. The crude snail lipid particles were ∼90 nm (Figure 2C). This value is slightly more than three times the diameter of LDLs (which are the aggregation inducers in FBS).[27] Next, we employed liquid chromatography-mass spectrometry (LC-MS) to evaluate the chemical composition of the solubilized snail lipid particles. Although analysis of crude snail serum extracts revealed the presence of over 800 lipids (see Table S1), the solubilized lipid particles did not contain the full array of serum lipids (i.e., some serum lipids resisted resuspension and were not delivered to the cells). Nonetheless, a complex mixture of major lipid classes including diglycerides, wax esters, triglycerides, and phospholipids was clearly incorporated into these aggregate-inducing particles (Figure 2D; Table S1). Therefore one (or many) lipids present in snail serum induce multicellular aggregation of *Capsaspora*.

We then asked if the aggregation activity was due to a minor component or a major lipid present in the extracted snail serum. To determine if a major lipid was responsible for the activity, we prepared a simplified lipid mixture from representative lipids of each of the major lipid classes present in the snail serum extract. The lipid mix, prepared from commercially available synthetic lipids, contained glyceryl dioleate (DG 18:1), glyceryl trioleate (TG 18:1), dioleoyl phosphatidylcholine (DOPC), 18:1/24:0 ceramide (Cer), and palmitoyl lysophosphatidylcholine (LPC 16:0). Despite being a large class represented in the extracted lipids, we did not include wax esters in this initial simple mix because we could not easily obtain short-tailed wax esters. We combined the five aforementioned lipids at approximately their natural ratio in snail serum and solubilized them by sonication into mixed-lipid particles. Remarkably, this simplified mixture induced aggregation in a dose-dependent manner with similar potency to the crude snail lipids (Figure 2E). We also validated the formation of lipid particles by TEM and DLS measurements as before, which revealed particles that were ∼50 nm in diameter (Figures 2F and 2G). We also determined the final lipid ratio in the particles by LC-MS to be slightly different than the original intended ratio (Figure 2H), yet all lipids were incorporated into the soluble particles. Thus, a simple mixture of the major snail serum lipids was sufficient to induce *Capsaspora* aggregation.

Then, to determine if a single lipid from snail serum was sufficient to induce aggregation, we tested each component of the active lipid mix individually. We added each lipid to *Capsaspora* (at the same concentration as in the simple lipid mix) and found pure DOPC lipids to be active, while no other lipids elicited an aggregation response (Figure 2I). The DOPC lipids induced robust aggregation in a dose dependent manner with an EC50 of 20 μg/mL (Figure 2J), which is about five times more potent than the extracted natural lipids from snail serum and the simplified lipid mix. We also validated the formation of lipid vesicles of ∼40 nm diameter with TEM and DLS (Figures 2K and 2L). Moreover, to determine if 20 μg/mL is a biologically relevant concentration, we quantified the amount of DOPC in snail serum using LC-MS. Based on spectral intensity normalized to an internal PC control, we estimated the concentration of DOPC in snail serum to be ∼2 μg/mL (∼10× lower than the EC50 of pure DOPC vesicles). Therefore, DOPC is likely not the sole inducer of aggregation present

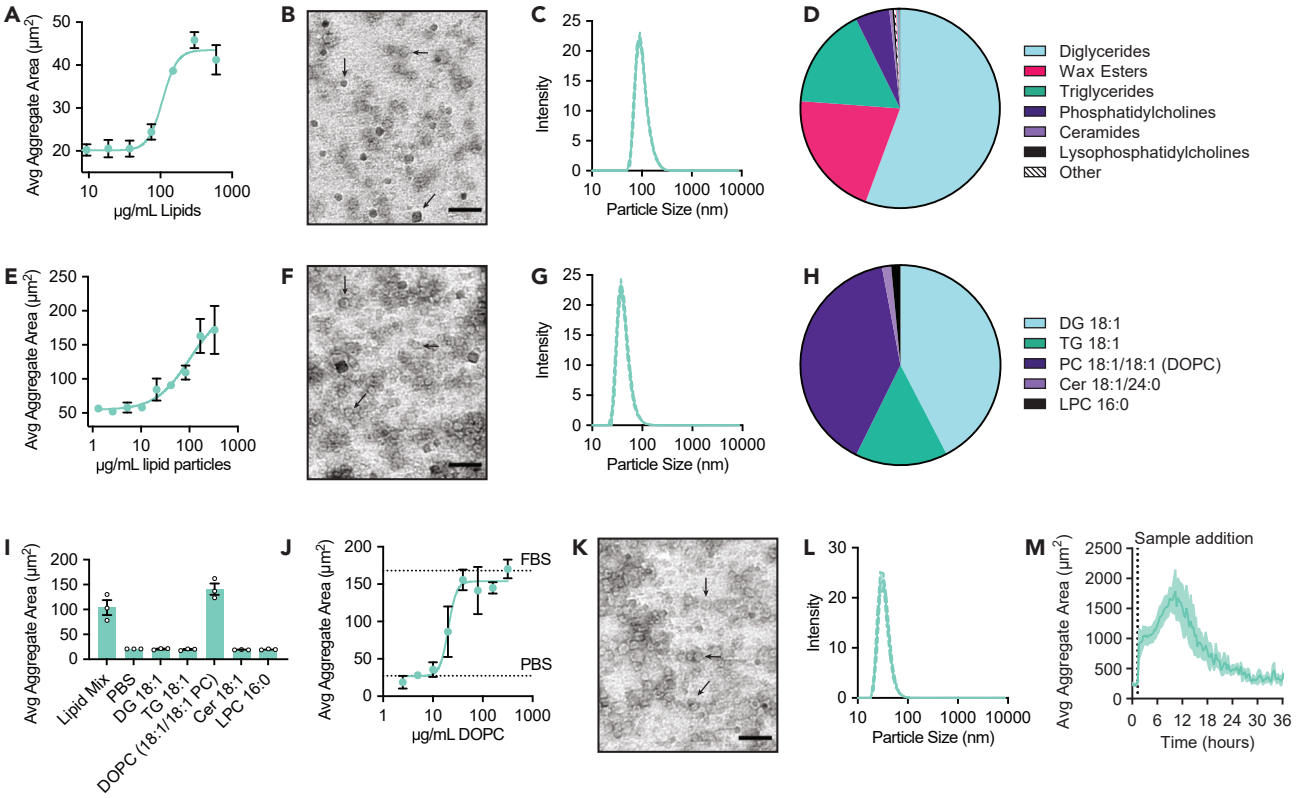

Figure 2. Lipids isolated from *Biomphalaria* snail serum induce aggregation

(A) Average area of aggregates induced by a dilution series of lipids isolated from snail serum and prepared into soluble emulsions. Area plotted as a function of lipid concentration in µg/mL. Lipids induced aggregation in a dose-dependent manner with an EC50 = 100 µg/mL.

(B) Representative TEM image of prepared crude snail serum lipid particles show active lipids were incorporated into particles with a range of sizes.

(C) Crude snail serum lipid particles were ~90 nm in diameter as measured by DLS.

(D) Pie chart of the major lipid classes present in the prepared and tested crude snail serum lipid particles. The most abundant lipid classes were diglycerides, wax esters, triglycerides, and phosphatidylcholines.

(E) Average area of aggregates induced by a simple mixture of synthetic lipids. The simple mix contained glyceryl dioleate (DG 18:1), glyceryl trioleate (TG 18:1), dioleoyl phosphatidylcholine (DOPC), 18:1/24:0 ceramide (Cer), and palmitoyl lysophosphatidylcholine (LPC 16:0). Lipids significantly induced aggregation at concentrations ~100 µg/mL, similarly to the extracted lipids.

(F) Representative TEM image of particles prepared using the simple synthetic lipid mix showed a range of sizes, much like the natural lipid preparation.

(G) Synthetic lipid mixture particles were ~50 nm in diameter as measured by DLS.

(H) Pie chart of the final lipid ratios included in the soluble synthetic lipid particles.

(I) Average area of aggregates induced by either the simple lipid mix or the individual lipids tested at the same concentration as present in the simple lipid mix. Of the individual lipids, only DOPC induced aggregation.

(J) Average area of aggregates induced by pure DOPC lipid vesicles. DOPC induced aggregation in a dose-dependent manner (EC50 = 20 µg/mL).

(K) Representative TEM image of DOPC vesicles.

(L) DOPC vesicles were ~40 nm in diameter as measured by DLS.

(M) The average aggregate area monitored every 20 min for 36 h after induction by 62.5 µg/mL of DOPC vesicles over time. For plots, means ± SEM (n = 3) are shown, and values from individual replicates are displayed with small circles. For microscopy images, scale bars are 100 nm, arrows highlight example particles.

in snail serum (e.g., other PCs in snail serum may contribute or other serum components may synergize with DOPC). In summary, pure DOPC, a lipid present in snail serum, is sufficient to induce *Capsaspora* multicellular aggregation; however, it is likely that other lipids also contribute to the phenotype.

Since the morphologies of FBS- and snail serum-induced aggregates had differed slightly, we assessed the morphology of DOPC-induced aggregates using the same quantifiable features measured in Figure S4. We found that DOPC-induced aggregates generally resembled those induced by FBS and/or snail serum, but their morphology depended on the concentration of DOPC (Figures S3E, S3F, and S6). This dependence of morphology on the identity and concentration of lipids suggested that *Capsaspora* aggregation morphology may differ depending on the exact hemolymph composition of its host.

Finally, we also monitored the aggregation dynamics induced by DOPC over time. We found that the dynamics of DOPC-induced aggregation were similar to the case of snail serum induction, although they formed quicker and dissipated earlier (Figure 2M; Video S2).

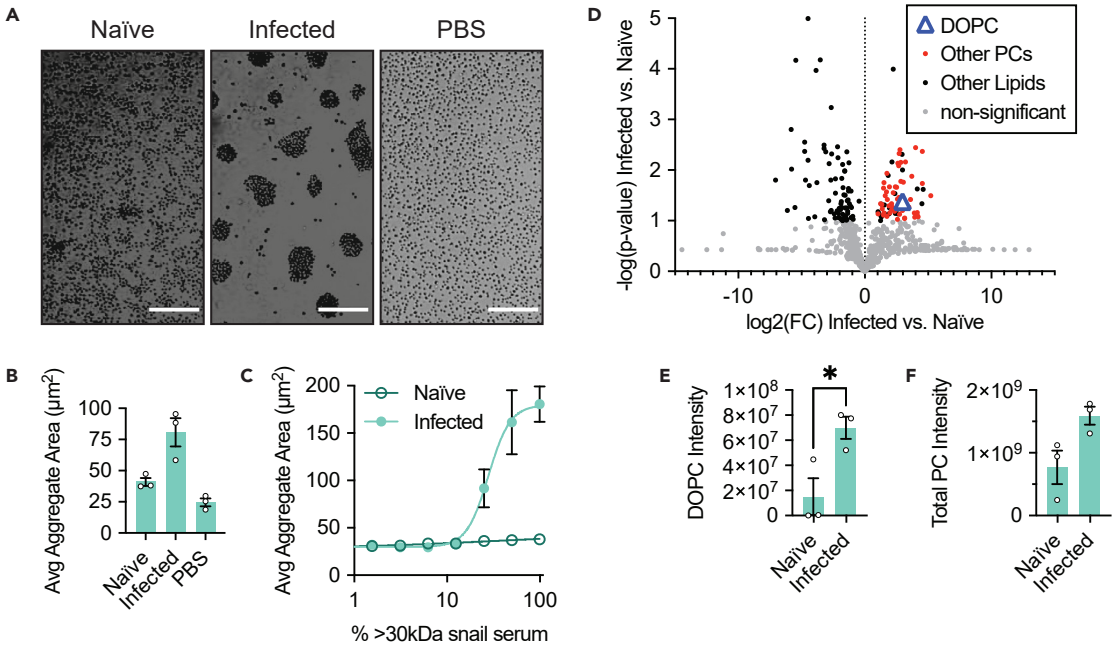

Figure 3. *Capsaspora* aggregates differently in response to serum from snails infected with schistosomes

(A) Representative images of *Capsaspora* cell aggregates induced by either 50% (v/v) >30 kDa serum from naive M-line snails, 50% (v/v) >30 kDa serum from schistosome-infected M-line snails, or 5% (v/v) PBS control. Cells were imaged 90 min after addition of inducers. Serum was collected from infected snails that were shedding cercariae 38 days post-exposure to schistosome miracidia. Uninfected snails were treated the same but not exposed to miracidia. Scale bars represent 100 µm.

(B) Average aggregate area of *Capsaspora* cells induced by snail serum samples compared to FBS and PBS controls.

(C) Dose-response curve of average aggregate area of cells induced by naive and infected sera. Infected serum induced aggregation significantly better than naive snail serum.

(D) Volcano plot showing the fold-change (FC) of individual lipids in naive vs. infected serum, detected by LC-MS/MS. The *p* values were calculated from analysis of 3 distinct batches of snails in each condition. Many PCs showed significant increases in the infected snails (see Table S1 for the full data).

(E) Comparison of DOPC $[M + H]^+$ intensity in each sample (Student's t test $p = 0.03$).

(F) Comparison of total identified PC $[M + H]^+$ intensity summed in each sample (Student's t test $p = 0.05$). For plots (B, C, E, and F), means ± SEM ($n = 3$) are shown, and values from individual replicates are displayed with small circles. An asterisk indicates $p < 0.05$ by a Student's t test.

Capsaspora responds to host infection with *Schistosoma mansoni*

Since aggregation was sensitive to the concentration of lipid inducers, we hypothesized that *Capsaspora* could sense physiological changes in its host snail that alter serum lipid levels. If so, its aggregation may be an adaptive response to these changes in its host physiology. Some lipids present in *Biomphalaria* serum are known to change in response to the snail's metabolic state. For example, snails fed different diets have exhibited different serum levels of triglycerides and other neutral lipids.[40,41] Furthermore, infection with parasites can alter lipid levels in *Biomphalaria* snails. For instance, serum cholesterol and triglyceride levels decrease in *B. glabrata* in response to infection with *Echinostoma paraensei*.[42] Triglycerides in the entire snail body also drop in response to infection with *Echinostoma caproni*.[43] Particularly of interest for our DOPC-induced aggregation, whole-snail PCs have been shown to double after 8 weeks of infection by *E. caproni*.[43] Therefore, to test if *Capsaspora* could sense schistosome-induced differences in host serum lipid composition, we harvested serum from naive outbred M-line *B. glabrata* snails as well as identical M-line snails that had been infected with 10 PR1 (Puerto Rico strain 1) *Schistosoma mansoni* miracidia 38 days prior (and were shedding mature schistosome cercaria). We tested the two sera for *Capsaspora* aggregation induction and observed a substantial difference between them (Figure 3A). Remarkably, serum from infected M-line snails induced *much greater aggregation* than the naive M-line snails, which showed comparatively little aggregation activity (Figures 3A and 3B). Moreover, the aggregation induced by serum from infected M-line snails was dose-dependent (Figure 3C).

To explain the difference, we hypothesized that the infected snail serum contained higher levels of DOPC and/or other PCs. Thus, we analyzed the lipid contents of each sample using liquid chromatography-tandem mass spectrometry (LC-MS/MS). Of the 800 lipids detected, we found 104 to be significantly different between the infected and naive snail sera (Figures 3D and S7; Table S1). Triglycerides and diglycerides generally decreased upon *S. mansoni* infection, which is consistent with previous studies of echinostome infections.[42,43] Also consistent with previous work of echinostome-infected snails,[43] *many of the PC lipids were significantly higher in the infected samples* (Figure 3D), *including DOPC* (Figure 3E). Furthermore, not a single detected PC was significantly depleted in the infected sample. Some abundant PCs were not substantially different between the two samples, rendering the sum of all PCs insignificantly different by a t test (Figure 3F).

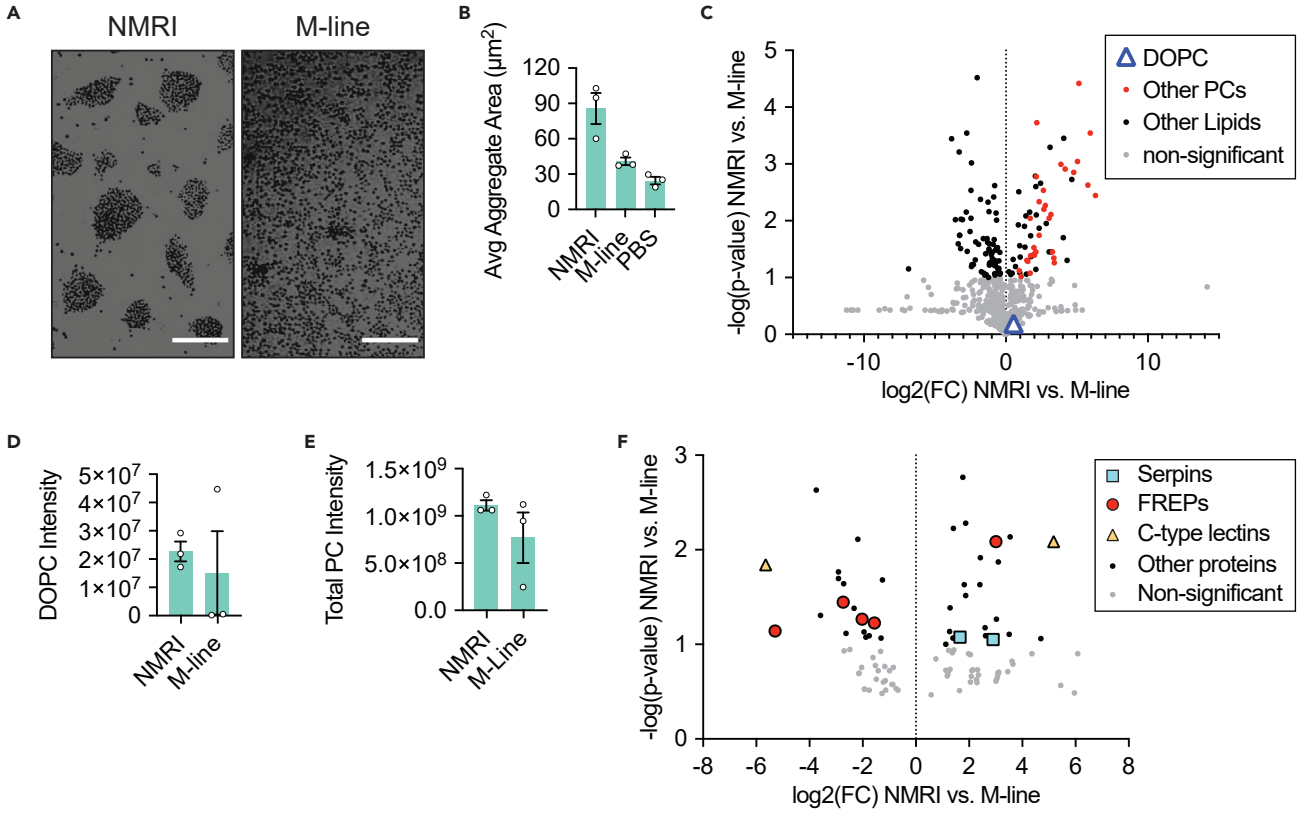

Figure 4. The *Capsaspora* aggregation phenotype discriminates between snail strains

(A) Representative images of *Capsaspora* aggregates induced by 50% (v/v) >30 kDa snail serum from naive NMRI snails and M-line snails. Cells were imaged 90 min after addition of inducers. Scale bars represent 100 µm.

(B) Average area of *Capsaspora* aggregates showed that naive NMRI snail serum is much more active than naive M-line serum.

(C) Volcano plot of the lipids identified by LC-MS/MS analysis of snail serum samples. Many PCs were higher in the active NMRI serum, but DOPC was not significantly different.

(D) Comparison of DOPC $[M + H]^+$ intensity in each sample (insignificant change by Student's t test).

(E) Comparison of total identified PC $[M + H]^+$ intensity summed in each sample (Student's t test $p = 0.2$).

(F) Volcano plot showing fold-change (FC) of individual proteins in naive NMRI vs. M-line snail sera determined by LC-MS/MS of tryptic peptides. The *p* values were calculated from analysis of 3 distinct batches of snails in each condition. 18 proteins were significantly higher in M-line than in NMRI and 23 proteins were significantly lower in M-line than NMRI. Notably, two serpins, five FREPs, and two C-type lectins were significantly different. For plots (B, D, and E), means ± SEM ($n = 3$) are shown, and values from individual replicates are displayed with small circles.

However, since several individual PCs were increased in the infected snails, it is plausible that the increased concentrations of a certain class of PCs in the infected snail serum caused the improved aggregation. Overall, these data show that *Capsaspora*'s aggregation phenotype is sensitive to schistosome-induced changes in host serum and that *Capsaspora* aggregation correlates with the serum concentration of DOPC and many other PCs.

Capsaspora responds differently to serum of different *Biomphalaria glabrata* strains

Unexpectedly, we observed that the aforementioned naive M-line snail serum failed to induce robust aggregation at any tested concentration (Figure 3C). This finding contrasted the previous results using serum from naive NMRI snails, which repeatedly induced robust aggregates (Figures 1F–1J). Moreover, this *Capsaspora* aggregation difference between M-line and NMRI snail sera persisted upon repeated inspection (Figures 4A and 4B). This difference could be due to the genotypes of the snails, or it could be due to snail age or different snail husbandry conditions (e.g., temperature, food, or snail density in tanks, see STAR Methods section). To explain the different aggregation potencies of the sera, we hypothesized that they might contain different levels of PC lipids. Specifically, the NMRI snail serum may have contained higher concentrations of PCs. Thus, we quantified the lipid content of serum from naive M-line and NMRI snail strains by LC-MS/MS analysis (Figure S7; Table S1). The two naive snail sera did not contain significantly different DOPC concentrations (Figures 4C and 4D). However, several other PCs were significantly higher in the NMRI serum compared to the M-line serum, and no PCs were lower in the NMRI serum (Figure 4C). Although the sum of PCs was insignificantly different between the samples (Figure 4E), it is plausible that a subset of specific PCs is

responsible for the observed difference in aggregation induction by our NMRI and M-line snails. Alternatively, we explored other explanations below.

We hypothesized that different *proteins* in the sera might also account for the different aggregation induction of the two naive sera. Two scenarios are possible: (1) inhibitory protein(s) that interfere with aggregation are lower in the NMRI serum or (2) activator protein(s) present in the NMRI snails are required for robust aggregation. To test these possibilities, we performed proteomics analysis of the two snail strains and found 18 proteins significantly higher in M-line serum and 23 proteins significantly higher in the NMRI serum (Figure 4F; Table S2). Two members of the serpin superfamily of serine protease inhibitors were significantly higher in the NMRI serum, suggesting that proteases might inhibit aggregation and that these protease inhibitors curtail that inhibition. Additionally, several fibrinogen-related proteins (FREPs) and a couple of C-type lectins were differentially abundant in the two snail sera. An FREP immune protein or lectin could bind to *Capsaspora* (or the lipid inducer itself) and block aggregation. Alternatively, one of these proteins may activate *Capsaspora* by somehow priming the cells to aggregate. Interestingly, subsequent proteomics analysis of the *infected* M-line snail serum also showed one FREP and one C-type lectin at levels similarly low to their levels in NMRI serum, demonstrating multiple inverse correlations between these specific proteins and aggregation induction activity (Figure S8; Table S2).

Further work is needed to confidently conclude if the PC differences are sufficient to explain the aggregation induction differences across host snail sera (or if other serum components inhibit or promote aggregation). Also, further work will determine if the differential aggregation induction is due to genomic differences between NMRI and M-line snails or environmental differences in snail husbandry. Nevertheless, these data indicate that *Capsaspora* may recognize other host differences beyond infection with schistosomes.

DISCUSSION

We have discovered that *Capsaspora* (a predator of parasitic schistosomes) can sense and respond to a specific chemical factor within its host snail's hemolymph. Namely, *Capsaspora* aggregates in response to a snail serum PC (Figures 5A and 5B). This discovery is the first example of a physiological response of *Capsaspora* to its host, which may inform how it colonizes its host and could therein exclude schistosome parasites.

Capsaspora was recently shown to aggregate in response to FBS *in vitro*.[27] However, mammalian serum is irrelevant to the expected natural life of *Capsaspora*, which has only been detected in *Biomphalaria* snails and once in fish feces (possibly caused by the fish eating snails).[44] Thus, our discovery that *Biomphalaria* tissue and hemolymph induce aggregation suggests that this aggregative phenotype *is an ecologically relevant response to a host environment*. As further support for the ecological significance of this phenotype, we found that all three existing isolated strains of *Capsaspora* aggregate in response to snail hemolymph—suggesting that *Capsaspora* aggregation is a widely conserved cellular response to the host environment.

As previously observed,[27] the aggregation phenotype within snail tissue was calcium-dependent. This observation may indicate the involvement of calcium-dependent cell-cell adhesion machinery[45] or the use of calcium as a secondary messenger[46] to regulate the aggregation response. Notably, snail hemolymph contains millimolar concentrations of calcium,[47] validating snail tissue as a suitable environment for aggregation.

We furthermore identified a single pure lipid from the snail hemolymph that is sufficient to induce aggregation: DOPC. Since PCs are major components of LDLs, we hypothesize that PCs are also the key aggregation inducers within LDLs, which were previously shown to induce aggregation.[27] Therefore, both FBS and snail serum may ultimately induce aggregation through the same PC-responsive pathway. Quantification of DOPC in snail serum revealed that its concentration was below the threshold level required for pure DOPC vesicles to quickly induce aggregation. Therefore, it is likely that other components in snail serum promote aggregation, as well. For example, other PCs may also induce aggregation—we are currently assessing the aggregation induction ability of a wide panel of phospholipids. Additionally, other serum components may synergize with DOPC to increase its potency. In fact, the aggregate morphologies upon DOPC induction differed some from those induced with whole snail serum, which also suggests that additional serum components contribute to aggregate formation. Since some *Capsaspora* mutants have exhibited similar differences in aggregation morphology, the unknown serum components may interact with these newly characterized pathways in *Capsaspora* to modify aggregate structure.[38]

Having identified the molecular cue of aggregation induction in snail serum, we asked whether *Capsaspora* would be able to use this cue to sense changes in the physiological state of its snail host. Other work has shown that certain lipid classes exhibit different abundance in snails under starvation and infection.[40–43] Remarkably, we found that schistosome-infected snails harbored elevated concentrations of DOPC (the aggregation inducer), and correspondingly, this serum more potently induced *Capsaspora* aggregation (Figures 5C and 5D). Therefore, it appears that *Capsaspora* can sense the infected state of its host snail and responds with more robust aggregation.

Furthermore, we discovered that sera from different snail strains grown under different conditions induced aggregation to different degrees. Uninfected NMRI snail serum induced aggregation far better than uninfected M-line serum. These strains have different genotypes, but they were also fed slightly different diets and housed in slightly different temperatures and densities (see STAR Methods). The NMRI snails were also larger (~12–17 mm) than the M-line snails (~8–10 mm). Any of these differences may provide unique chemical environments within the two naive snails. Surprisingly, we found no significant difference in the concentrations of DOPC between the two snail strains. However, other PCs were significantly higher in NMRI serum (and none were higher in M-line serum). Therefore, the induction ability may still rely on a threshold concentration of certain PCs. Alternatively, aggregation may be induced or inhibited by other factors that differ between the strains. The serum proteomes of the two snail strains revealed different levels of FREPs. These proteins serve as immune effectors in snails[48] and are known to differ in expression across inbred lines[49] and during infections.[50] M-line snails may produce specific FREPs that block *Capsaspora*

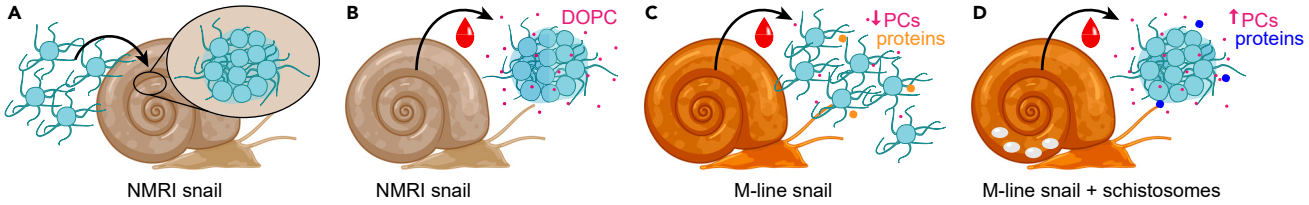

Figure 5. Overview of *Capsaspora* aggregative response to host and upon distinct host-pathogen interactions

(A) When introduced to NMRI snail tissue, *Capsaspora* aggregates.

(B) NMRI snail serum also induces *Capsaspora* aggregation, and the serum lipids are responsible for the aggregation—particularly dioleoyl phosphatidylcholine (DOPC).

(C and D) M-line snail serum fails to induce robust *Capsaspora* aggregates *in vitro* unless the snails have been pre-infected with schistosomes. Schistosome infection increases the concentration of DOPC (and other PCs) and alters the serum proteome.

aggregation by preventing its interaction with DOPC or by directly inhibiting its cell-cell contacts. If this hypothesis proves true, it is notable that some FREPs were also depleted in the infected M-line serum, including one that was depleted in the active NMRI serum. Therefore, the increased aggregation in infected serum could be *both* due to increased DOPC concentrations *and* decreased concentrations of certain FREPs. Alternatively, the NMRI FREPs may play a role in promoting DOPC-induced aggregation.[51] Serpin protease inhibitors, a class of proteins that have previously been investigated for their role in host-pathogen interactions,[52] were also increased in the aggregation-inducing NMRI serum, possibly indicating an anti-aggregation effect by proteases. Ultimately, the chemical composition of sera from different snail strains grown in different laboratory conditions yielded remarkably different *Capsaspora* aggregation, which indicates that *Capsapsora* may be able to distinguish between potential hosts based on their chemical factors.

In total, these discoveries raise the question of why *Capsaspora* aggregates inside its snail host. Furthermore, it is curious what benefit *Capsaspora* would gain from aggregating more in schistosome-infected snails than in naive snails. The potential benefits of multicellular forms are myriad,[53–55] but we mention a few specifically here. First, diverse microbes form multicellular adhesive phenotypes to remain in favorable environments.[53–55] For *Capsaspora*, the large aggregates may localize to certain favorable tissues or avoid excretion from the host. A second potential benefit is efficient utilization of secreted exoenzymes. Like many osmotrophic microbes, *Capsaspora* is believed to secrete enzymes to liberate soluble nutrients.[28] As more cells co-localize, they benefit from each other's "common goods" and feed more efficiently. This logic has explained the frequent exoenzyme regulation by quorum sensing (or "diffusion sensing") in bacteria.[56] Finally, aggregation may protect *Capsaspora* from the snail immune system. Multicellular growth is known to protect symbiotic and free-living microbes from predation.[57–60] Because snail hemolymph contains immune cells (hemocytes) that can engulf prey[61] as well as release toxic soluble factors,[62,63] *Capsaspora* aggregation may afford protection from these insults. Why *Capsaspora* would particularly benefit from aggregation in schistosome-infected snails is also unclear. Perhaps the elevated PC levels indicate a more nutrient-rich environment that favors adhesion and cooperative feeding. Alternatively, higher PC concentrations may indicate an elevated immune state that necessitates protective aggregation.

It is tempting to speculate that the different aggregation responses to sera from different snails will lead to different abilities of *Capsaspora* to colonize those snails. Because serum-induced aggregation is conserved across all existing isolates of *Capsaspora*, the phenotype is likely important for its natural fitness in the snail. However, further work is required to determine the necessity of aggregation for snail colonization. If aggregation indeed promotes colonization, then *Capsaspora* may fare better in schistosome-infected snails and in NMRI snails than in uninfected M-line snails. In ongoing work, we are testing this hypothesized dependence of *Capsaspora* colonization on snail strain and infection status.

Lastly, aside from its symbiosis with snails, *Capsaspora* is also an important model for studying the evolution of multicellular phenotypes in animals.[23] It is one of the closest living relatives of animals and contains many genes that are important for cell-cell adhesion and signaling in animals.[19] Furthermore, Ruiz-Trillo and co-workers have proposed that *Capsaspora*-like aggregation in the unicellular ancestor of animals may have been a pivotal step in the evolution of the first multicellular animals.[64] Specifically, cell aggregation may have been the first step to establish obligate multicellular animals (instead of, or in addition to, incomplete separation of cells after clonal cell division). Therefore, dissecting how and why aggregation occurs in *Capsaspora* may illuminate potential mechanisms of aggregative multicellularity in the unicellular ancestor of animals and in the earliest animals. Now that a pure chemical inducer is known, it can be leveraged into biochemical and genetic experiments to determine how *Capsaspora* regulates its multicellularity, both *in vivo* and *in vitro*. Comparative genomics of the regulatory pathway(s) across animals and non-animal holozoans can then assess the potential ancestry of regulated cell-cell adhesion phenotypes in animals. Along this line, it will also be informative to determine if *Capsaspora*'s relatives (e.g., *Pigoraptor* spp.,[65] *Ministeria vibrans*,[66] *Txikispora philomaios*,[67] and *Tunicaraptor unikontum*[68]; see Figure S9) also aggregate in response to PCs, especially given that they exhibit a range of free-living and parasitic lifestyles. If so, this response to PCs may be ancestral, predating *Capsaspora*'s symbiosis with snails and perhaps even predating the divergence of animals from their unicellular holozoan ancestor. Overall, by more deeply elucidating the mechanism of this lipid-induced aggregative response and the breadth of its conservation across phyla, we (and others) can discern the significance of lipids in regulating multicellular behaviors in the evolution of animals.

Limitations of the study

Although we have identified a phenotypic response of *Capsaspora* to host cellular components, we have not established the significance of this response to *Capsaspora*'s viability in its host. We hypothesize that the aggregation behavior is important for *Capsaspora*'s ability to colonize and persist in its host, but this hypothesis awaits further evaluation. Furthermore, although *Capsaspoa* can kill schistosomes *in vitro*,[12,28] it has not yet been shown that *Capsaspora* kills schistosomes within snails. Toward this end, we are improving in-snail imaging to assess aggregation in living snails within their shells. Efforts are also underway to assess colonization of different snail strains with different husbandry conditions. Improved methods of colonization and detection will be necessary to evaluate long-term *in vivo* aggregation and its potential significance for colonization of snails. Then, studies can proceed to evaluate the impact of robust *Capsaspora* colonization on schistosome development and shedding from *Capsaspora*-colonized snails.

Conclusion

In sum, we discovered that a snail symbiont that is capable of killing human parasites can adapt its behavior to its host snail environment. Namely, the symbiont *Capsaspora* forms multicellular aggregates in *B. glabrata* snail host tissue and hemolymph. *Capsaspora* senses at least one specific lipid (DOPC) from its host serum and may use the concentration of this lipid and its analogs to sense the physiological state and genotype of its host. Because this response is conserved across several symbiont isolates, it is likely significant for the natural life of *Capsaspora*. These findings pave the way for further work to investigate the persistence of *Capsaspora* within the host, the potential importance of *Capsaspora* aggregation for its ability to colonize snails, and ultimately, this symbiont's ability to limit the proliferation and spread of parasitic schistosomes from snails.

RESOURCE AVAILABILITY

Lead contact

Further information and requests should be directed to the lead contact, Joseph P. Gerdt (jpgerdt@iu.edu).

Materials availability

The plasmid generated in this study has been deposited to Addgene (pJG01, #213505).

Data and code availability

- Proteomics and lipidomics raw data from this study have been deposited in MassIVE (MSV000094051; MSV000094067).
- Any other raw data from this study are available from the lead contact upon reasonable request.
- This study does not report original code.
- Any additional information required to reanalyze the data reported in this paper is available from the lead contact upon request.

ACKNOWLEDGMENTS

We thank the Schistosomiasis Resource Center for provision of snails and schistosomes. NMRI snails were provided by the Schistosomiasis Resource Center of the Biomedical Research Institute (Rockville, MD) through NIH-NIAID Contract HHSN272201700014I NIH: *B. glabrata* (NMRI). We thank Margaret Mentink-Kane and André Miller for instruction on rearing snails and collecting hemolymph. We thank Timothy Yoshino for advice and initial provision of snail serum. We thank Eric Loker and Chris Bayne for advice. We thank the Light Microscopy Center at Indiana University for support in image acquisition and analysis (funding provided by the NIH grant NIH1S10OD024988-01). We also thank the Indiana University Nanoscale Characterization Facility, Electron Microscopy Center, and Laboratory for Biological Mass Spectrometry for use of their instruments. We thank Jon Trinidad for proteomics assistance and John Asara for lipidomics assistance. We thank Pranav Danthi for use of the Incucyte imager and Andrew Zelhof for assistance in injecting *Capsaspora* into snails. We thank Jonathan Phillips for advice with *Capsaspora* transfection. We thank Iñaki Ruiz-Trillo for feedback on the manuscript. We also thank the entire Gerdt lab for insights and support that helped advance this project. This work was supported by the National Institutes of Health (R35GM138376) to J.P.G. as well as NIH grants (R37AI101438 and P30GM110907). R.Q.K. was supported by an NIH training grant (T32GM131994). The content of this paper is solely the responsibility of the authors and does not necessarily represent the official views of the National Institutes of Health.

AUTHOR CONTRIBUTIONS

Conceptualization, R.Q.K., N.R.-R., and J.P.G.; methodology, R.Q.K., M.R.L., C.G., and J.P.G.; investigation, R.Q.K., E.B.G., M.R.L., M.C.S., C.G., and L.P.B.; resources, J.M. and W.S.D.; writing – original draft, R.Q.K. and J.P.G.; writing – review & editing, R.Q.K., M.R.L., N.R.-R., and J.P.G.; visualization – R.Q.K. and J.P.G.; supervision, J.P.G.; funding acquisition, J.P.G.

DECLARATION OF INTERESTS

The authors declare no competing interests.

STAR★METHODS

Detailed methods are provided in the online version of this paper and include the following:

- KEY RESOURCES TABLE
- EXPERIMENTAL MODEL AND STUDY PARTICIPANT DETAILS
  - Capsaspora *owczarzaki* cell cultures (strain ATCC30864)
  - M-line Capsaspora *owczarzaki* cell cultures (strain ATCC50973)
  - Salvador *Capsaspora owczarzaki* cell cultures (strain ATCC50974)

SUPPLEMENTAL INFORMATION

Supplemental information can be found online at https://doi.org/10.1016/j.isci.2024.110724.

Received: April 6, 2024
Revised: June 28, 2024
Accepted: August 8, 2024
Published: August 14, 2024

REFERENCES

1. McFall-Ngai, M., Hadfield, M.G., Bosch, T.C.G., Carey, H.V., Domazet-Lošo, T., Douglas, A.E., Dubilier, N., Eberl, G., Fukami, T., Gilbert, S.F., et al. (2013). Animals in a bacterial world, a new imperative for the life sciences. Proc. Natl. Acad. Sci. USA *110*, 3229–3236. https://doi.org/10.1073/pnas.1218525110.
2. Drew, G.C., Stevens, E.J., and King, K.C. (2021). Microbial evolution and transitions along the parasite–mutualist continuum. Nat. Rev. Microbiol. *19*, 623–638. https://doi.org/10.1038/s41579-021-00550-7.
3. del Campo, J., Bass, D., and Keeling, P.J. (2020). The eukaryome: Diversity and role of microeukaryotic organisms associated with animal hosts. Funct. Ecol. *34*, 2045–2054. https://doi.org/10.1111/1365-2435.13490.
4. Fisher, M.C., Henk, D.A., Briggs, C.J., Brownstein, J.S., Madoff, L.C., McCraw, S.L., and Gurr, S.J. (2012). Emerging fungal threats to animal, plant and ecosystem health. Nature *484*, 186–194. https://doi.org/10.1038/nature10947.
5. Du, H., Bing, J., Hu, T., Ennis, C.L., Nobile, C.J., and Huang, G. (2020). *Candida auris*: Epidemiology, biology, antifungal resistance, and virulence. PLoS Pathog. *16*, e1008921. https://doi.org/10.1371/journal.ppat.1008921.
6. Akhoundi, M., Kuhls, K., Cannet, A., Votýpka, J., Marty, P., Delaunay, P., and Sereno, D. (2016). A historical overview of the classification, evolution, and dispersion of Leishmania parasites and sandflies. PLoS Neglect. Trop. Dis. *10*, e0004349. https://doi.org/10.1371/journal.pntd.0004349.
7. Cowman, A.F., Healer, J., Marapana, D., and Marsh, K. (2016). Malaria: Biology and disease. Cell *167*, 610–624. https://doi.org/10.1016/j.cell.2016.07.055.
8. Lin, S., Cheng, S., Song, B., Zhong, X., Lin, X., Li, W., Li, L., Zhang, Y., Zhang, H., Ji, Z., et al. (2015). The *Symbiodinium kawagutii* genome illuminates dinoflagellate gene expression and coral symbiosis. Science *350*, 691–694. https://doi.org/10.1126/science.aad0408.
9. Kittelmann, S., Devente, S.R., Kirk, M.R., Seedorf, H., Dehority, B.A., and Janssen, P.H. (2015). Phylogeny of intestinal ciliates, including *Charonina ventriculi*, and comparison of microscopy and 18S rRNA gene pyrosequencing for rumen ciliate community structure analysis. Appl. Environ. Microbiol. *81*, 2433–2444. https://doi.org/10.1128/AEM.03697-14.
10. Chudnovskiy, A., Mortha, A., Kana, V., Kennard, A., Ramirez, J.D., Rahman, A., Remark, R., Mogno, I., Ng, R., Gnjatic, S., et al. (2016). Host-protozoan interactions protect from mucosal infections through activation of the inflammasome. Cell *167*, 444–456.e14. https://doi.org/10.1016/j.cell.2016.08.076.
11. Hertel, L.A., Bayne, C.J., and Loker, E.S. (2002). The symbiont *Capsaspora owczarzaki*, nov. gen. nov. sp., isolated from three strains of the pulmonate snail *Biomphalaria glabrata* is related to members of the Mesomycetozoea. Int. J. Parasitol. *32*, 1183–1191. https://doi.org/10.1016/S0020-7519(02)00066-8.
12. Stibbs, H.H., Owczarzak, A., Bayne, C.J., and DeWan, P. (1979). Schistosome sporocyst-killing amoebae isolated from *Biomphalaria glabrata*. J. Invertebr. Pathol. *33*, 159–170. https://doi.org/10.1016/0022-2011(79)90149-6.
13. Harry, H.W., and Aldrich, D.V. (1958). The ecology of *Australorbis glabratus* in Puerto Rico. Bull. World Health Organ. *18*, 819–832.
14. Stirewalt, M.A. (1954). Effect of snail maintenance temperatures on development of *Schistosoma mansoni*. Exp. Parasitol. *3*, 504–516. https://doi.org/10.1016/0014-4894(54)90046-6.
15. Pimentel, D. (1957). Life history of *Australorbis glabratus*, the intermediate snail host of *Schistosoma mansoni* in Puerto Rico. Ecology *38*, 576–580. https://doi.org/10.2307/1943122.
16. Lewis, F.A., Stirewalt, M.A., Souza, C.P., and Gazzinelli, G. (1986). Large-scale laboratory maintenance of *Schistosoma mansoni*, with observations on three schistosome/snail host combinations. J. Parasitol. *72*, 813–829.
17. Adema, C.M., Bayne, C.J., Bridger, J.M., Knight, M., Loker, E.S., Yoshino, T.P., and Zhang, S.-M. (2012). Will all scientists working on snails and the diseases they transmit please stand up? PLoS Negl. Trop. Dis. *6*, e1835. https://doi.org/10.1371/journal.pntd.0001835.
18. Sebé-Pedrós, A., Ballaré, C., Parra-Acero, H., Chiva, C., Tena, J.J., Sabidó, E., Gómez-Skarmeta, J.L., Di Croce, L., and Ruiz-Trillo, I. (2016). The dynamic regulatory genome of *Capsaspora* and the origin of animal multicellularity. Cell *165*, 1224–1237. https://doi.org/10.1016/j.cell.2016.03.034.
19. Ferrer-Bonet, M., and Ruiz-Trillo, I. (2017). Capsaspora owczarzaki. Curr. Biol. *27*, R829–

R830. https://doi.org/10.1016/j.cub.2017.05.074.

20. Pérez-Posada, A., Dudin, O., Ocaña-Pallarès, E., Ruiz-Trillo, I., and Ondracka, A. (2020). Cell cycle transcriptomics of *Capsaspora* provides insights into the evolution of cyclin-CDK machinery. PLoS Genet. *16*, e1008584. https://doi.org/10.1371/journal.pgen.1008584.
21. Sebé-Pedrós, A., Peña, M.I., Capella-Gutiérrez, S., Antó, M., Gabaldón, T., Ruiz-Trillo, I., and Sabidó, E. (2016). High-throughput proteomics reveals the unicellular roots of animal phosphosignaling and cell differentiation. Dev. Cell *39*, 186–197. https://doi.org/10.1016/j.devcel.2016.09.019.
22. Suga, H., Chen, Z., de Mendoza, A., Sebé-Pedrós, A., Brown, M.W., Kramer, E., Carr, M., Kerner, P., Vervoort, M., Sánchez-Pons, N., et al. (2013). The *Capsaspora* genome reveals a complex unicellular prehistory of animals. Nat. Commun. *4*, 2325. https://doi.org/10.1038/ncomms3325.
23. Sebé-Pedrós, A., Irimia, M., del Campo, J., Parra-Acero, H., Russ, C., Nusbaum, C., Blencowe, B.J., and Ruiz-Trillo, I. (2013). Regulated aggregative multicellularity in a close unicellular relative of metazoa. Elife *2*, e01287. https://doi.org/10.7554/eLife.01287.
24. Parra-Acero, H., Harcet, M., Sánchez-Pons, N., Casacuberta, E., Brown, N.H., Dudin, O., and Ruiz-Trillo, I. (2020). Integrin-mediated adhesion in the unicellular holozoan *Capsaspora owczarzaki*. Curr. Biol. *30*, 4270–4275.e4274. https://doi.org/10.1016/j.cub.2020.08.015.
25. Parra-Acero, H., Ros-Rocher, N., Perez-Posada, A., Kożyczkowska, A., Sánchez-Pons, N., Nakata, A., Suga, H., Najle, S.R., and Ruiz-Trillo, I. (2018). Transfection of *Capsaspora owczarzaki*, a close unicellular relative of animals. Development *145*, dev162107. https://doi.org/10.1242/dev.162107.
26. Phillips, J.E., Santos, M., Konchwala, M., Xing, C., and Pan, D. (2022). Genome editing in the unicellular holozoan *Capsaspora owczarzaki* suggests a premetazoan role for the Hippo pathway in multicellular morphogenesis. Elife *11*, e77598. https://doi.org/10.7554/eLife.77598.
27. Ros-Rocher, N., Kidner, R.Q., Gerdt, C., Davidson, W.S., Ruiz-Trillo, I., and Gerdt, J.P. (2023). Chemical factors induce aggregative multicellularity in a close unicellular relative of animals. Proc. Natl. Acad. Sci. USA *120*, e2216668120. https://doi.org/10.1073/pnas.2216668120.
28. Owczarzak, A., Stibbs, H.H., and Bayne, C.J. (1980). The destruction of *Schistosoma mansoni* mother sporocysts *in vitro* by amoebae isolated from *Biomphalaria glabrata*: an ultrastructural study. J. Invertebr. Pathol. *35*, 26–33. https://doi.org/10.1016/0022-2011(80)90079-8.
29. Utarini, A., Indriani, C., Ahmad, R.A., Tantowijoyo, W., Arguni, E., Ansari, M.R., Supriyati, E., Wardana, D.S., Meitika, Y., Ernesia, I., et al. (2021). Efficacy of *Wolbachia*-infected mosquito deployments for the control of dengue. N. Engl. J. Med. *384*, 2177–2186. https://doi.org/10.1056/NEJMoa2030243.
30. Moreira, L.A., Iturbe-Ormaetxe, I., Jeffery, J.A., Lu, G., Pyke, A.T., Hedges, L.M., Rocha, B.C., Hall-Mendelin, S., Day, A., Riegler, M., et al. (2009). A *Wolbachia* symbiont in *Aedes aegypti* limits infection with dengue, chikungunya, and *Plasmodium*. Cell *139*, 1268–1278. https://doi.org/10.1016/j.cell.2009.11.042.
31. Bian, G., Joshi, D., Dong, Y., Lu, P., Zhou, G., Pan, X., Xu, Y., Dimopoulos, G., and Xi, Z. (2013). *Wolbachia* invades *Anopheles stephensi* populations and induces refractoriness to *Plasmodium* infection. Science *340*, 748–751. https://doi.org/10.1126/science.1236192.
32. Evan Secor, W. (2014). Water-based interventions for schistosomiasis control. Pathog. Glob. Health *108*, 246–254. https://doi.org/10.1179/2047773214y.0000000149.
33. McCullough, F.S., Gayral, P., Duncan, J., and Christie, J.D. (1980). Molluscicides in schistosomiasis control. Bull. World Health Organ. *58*, 681–689.
34. Laidemitt, M.R., Anderson, L.C., Wearing, H.J., Mutuku, M.W., Mkoji, G.M., and Loker, E.S. (2019). Antagonism between parasites within snail hosts impacts the transmission of human schistosomiasis. Elife *8*, e50095. https://doi.org/10.7554/eLife.50095.
35. Bayne, C.J. (1982). Lectin-induced mitogenesis of cytotoxic amebae (Nuclearia) isolated from *Biomphalaria glabrata* (Mollusca: Gastropoda). Dev. Comp. Immunol. *6*, 369–373. https://doi.org/10.1016/S0145-305X(82)80020-7.
36. Buddenborg, S.K., Bu, L., Zhang, S.-M., Schilkey, F.D., Mkoji, G.M., and Loker, E.S. (2017). Transcriptomic responses of *Biomphalaria pfeifferi* to *Schistosoma mansoni*: Investigation of a neglected African snail that supports more *S. mansoni* transmission than any other snail species. PLoS Negl. Trop. Dis. *11*, e0005984. https://doi.org/10.1371/journal.pntd.0005984.
37. Kidner, R.Q., Goldstone, E.B., Rodefeld, H.J., Brokaw, L.P., Gonzalez, A.M., Ros-Rocher, N., and Gerdt, J.P. (2024). Exogenous lipid vesicles induce endocytosis-mediated cellular aggregation in a close unicellular relative of animals. Preprint at bioRxiv. https://doi.org/10.1101/2024.05.14.593945.
38. Phillips, J.E., and Pan, D. (2024). The Hippo kinase cascade regulates a contractile cell behavior and cell density in a close unicellular relative of animals. Elife *12*, RP90818. https://doi.org/10.7554/eLife.90818.
39. Baker, M.E. (1988). Is vitellogenin an ancestor of apolipoprotein B-100 of human low-density lipoprotein and human lipoprotein lipase? Biochem. J. *255*, 1057–1060. https://doi.org/10.1042/bj2551057.
40. Fried, B., Cahn-Hidalgo, D., Fujino, T., and Sherma, J. (1991). Diet-induced differences in the distribution of neutral lipids in selected organs of *Biomphalaria glabrata* (Gastropoda: Planorbidae) as determined by thin-layer chromatography and light and electron microscopy. Trans. Am. Microsc. Soc. *110*, 163–171. https://doi.org/10.2307/3226752.
41. Aloisi, J.D., Fried, B., and Sherma, J. (1991). Reversal of dietary-induced hyperlipidemia in *Biomphalaria glabrata* (Gastropoda). Comp. Biochem. Physiol. A Comp. Physiol. *100*, 203–204. https://doi.org/10.1016/0300-9629(91)90208-t.
42. Tunholi-Alves, V.M., Tunholi, V.M., Gôlo, P., Lustrino, D., Maldonado, A., Jr., Bittencourt, V.R.E.P., Rodrigues, M.d.L.d.A., and Pinheiro, J. (2011). Lipid levels in *Biomphalaria glabrata* infected with different doses of *Echinostoma paraensei* miracidia. Exp. Parasitol. *128*, 212–216. https://doi.org/10.1016/j.exppara.2011.03.009.
43. Bandstra, S.R., Fried, B., and Sherma, J. (2006). High-performance thin-layer chromatographic analysis of neutral lipids and phospholipids in *Biomphalaria glabrata* patently infected with *Echinostoma caproni*. Parasitol. Res. *99*, 414–418. https://doi.org/10.1007/s00436-006-0180-5.
44. Ray, C.L., Abernathy, J.W., Green, B.W., Rivers, A.R., Schrader, K.K., Rawles, S.D., McEntire, M.E., Lange, M.D., and Webster, C.D. (2024). Effect of dietary phytase on water and fecal prokaryotic and eukaryotic microbiomes in a hybrid tilapia (*Oreochromis aureus* x *O. niloticus*) mixotrophic biofloc production system. Aquaculture *581*, 740433. https://doi.org/10.1016/j.aquaculture.2023.740433.
45. Kemler, R., Ozawa, M., and Ringwald, M. (1989). Calcium-dependent cell adhesion molecules. Curr. Opin. Cell Biol. *1*, 892–897. https://doi.org/10.1016/0955-0674(89)90055-0.
46. Clapham, D.E. (2007). Calcium signaling. Cell *131*, 1047–1058. https://doi.org/10.1016/j.cell.2007.11.028.
47. Machałowski, T., and Jesionowski, T. (2020). Hemolymph of molluscan origin: from biochemistry to modern biomaterials science. Appl. Phys. A *127*, 1–22. https://doi.org/10.1007/s00339-020-04166-1.
48. Hanington, P.C., and Zhang, S.M. (2011). The primary role of fibrinogen-related proteins in invertebrates is defense, not coagulation. J. Innate Immun. *3*, 17–27. https://doi.org/10.1159/000321882.
49. Adema, C.M. (2015). Fibrinogen-related proteins (FREPs) in mollusks. Results Probl. Cell Differ. *57*, 111–129. https://doi.org/10.1007/978-3-319-20819-0_5.
50. Lu, L., Loker, E.S., Adema, C.M., Zhang, S.M., and Bu, L. (2020). Genomic and transcriptional analysis of genes containing fibrinogen and IgSF domains in the schistosome vector *Biomphalaria glabrata*, with emphasis on the differential responses of snails susceptible or resistant to *Schistosoma mansoni*. PLoS Negl. Trop. Dis. *14*, e0008780. https://doi.org/10.1371/journal.pntd.0008780.
51. Faizullin, D., Valiullina, Y., Salnikov, V., and Zuev, Y. (2020). Direct interaction of fibrinogen with lipid microparticles modulates clotting kinetics and clot structure. Nanomedicine. *23*, 102098. https://doi.org/10.1016/j.nano.2019.102098.
52. Bao, J., Pan, G., Poncz, M., Wei, J., Ran, M., and Zhou, Z. (2018). Serpin functions in host-pathogen interactions. PeerJ *6*, e4557. https://doi.org/10.7717/peerj.4557.
53. Herron, M.D., Conlin, P.L., and Ratcliff, W.C. (2022). The Evolution of Multicellularity, First edition (CRC Press)).
54. Lyons, N.A., and Kolter, R. (2015). On the evolution of bacterial multicellularity. Curr. Opin. Microbiol. *24*, 21–28. https://doi.org/10.1016/j.mib.2014.12.007.
55. Bonner, J.T. (1998). The origins of multicellularity. Integr. Biol. *1*, 27–36. https://doi.org/10.1002/(SICI)1520-6602(1998)1:1<27::AID-INBI4>3.0.CO;2-6.
56. Darch, S.E., West, S.A., Winzer, K., and Diggle, S.P. (2012). Density-dependent fitness benefits in quorum-sensing bacterial populations. Proc. Natl. Acad. Sci. USA *109*, 8259–8263. https://doi.org/10.1073/pnas.1118131109.
57. Justice, S.S., Hunstad, D.A., Cegelski, L., and Hultgren, S.J. (2008). Morphological plasticity as a bacterial survival strategy. Nat. Rev.

Microbiol. *6*, 162–168. https://doi.org/10.1038/nrmicro1820.

58. Roilides, E., Simitsopoulou, M., Katragkou, A., and Walsh, T.J. (2015). How biofilms evade host defenses. Microbiol. Spectr. *3*, 287–300. https://doi.org/10.1128/microbiolspec.mb-0012-2014.
59. Herron, M.D., Borin, J.M., Boswell, J.C., Walker, J., Chen, I.C.K., Knox, C.A., Boyd, M., Rosenzweig, F., and Ratcliff, W.C. (2019). De novo origins of multicellularity in response to predation. Sci. Rep. *9*, 2328. https://doi.org/10.1038/s41598-019-39558-8.
60. Kapsetaki, S.E., and West, S.A. (2019). The costs and benefits of multicellular group formation in algae. Evolution *73*, 1296–1308. https://doi.org/10.1111/evo.13712.
61. Loker, E.S., Bayne, C.J., Buckley, P.M., and Kruse, K.T. (1982). Ultrastructure of encapsulation of *Schistosoma mansoni* mother sporocysts by hemocytes of juveniles of the 10-R2 strain of *Biomphalaria glabrata*. J. Parasitol. *68*, 84–94.
62. Castillo, M.G., Humphries, J.E., Mourão, M.M., Marquez, J., Gonzalez, A., and Montelongo, C.E. (2020). *Biomphalaria glabrata* immunity: Post-genome advances. Dev. Comp. Immunol. *104*, 103557. https://doi.org/10.1016/j.dci.2019.103557.
63. Galinier, R., Portela, J., Moné, Y., Allienne, J.F., Henri, H., Delbecq, S., Mitta, G., Gourbal, B., and Duval, D. (2013). Biomphalysin, a new β pore-forming toxin involved in *Biomphalaria glabrata* immune defense against *Schistosoma mansoni*. PLoS Pathog. *9*, e1003216. https://doi.org/10.1371/journal.ppat.1003216.
64. Ruiz-Trillo, I., Kin, K., and Casacuberta, E. (2023). The origin of metazoan multicellularity: a potential microbial black swan event. Annu. Rev. Microbiol. *77*, 499–516. https://doi.org/10.1146/annurev-micro-032421-120023.
65. Hehenberger, E., Tikhonenkov, D.V., Kolisko, M., del Campo, J., Esaulov, A.S., Mylnikov, A.P., and Keeling, P.J. (2017). Novel predators reshape holozoan phylogeny and reveal the presence of a two-component signaling system in the ancestor of animals. Curr. Biol. *27*, 2043–2050.e6. https://doi.org/10.1016/j.cub.2017.06.006.
66. Tong, S.M. (1997). Heterotrophic flagellates and other protists from Southampton Water, U.K. Ophelia *47*, 71–131. https://doi.org/10.1080/00785236.1997.10427291.
67. Urrutia, A., Mitsi, K., Foster, R., Ross, S., Carr, M., Ward, G.M., van Aerle, R., Marigomez, I., Leger, M.M., Ruiz-Trillo, I., et al. (2022). *Txikispora philomaios* n. sp., n. g., a micro-eukaryotic pathogen of amphipods, reveals parasitism and hidden diversity in Class Filasterea. J. Eukaryot. Microbiol. *69*, e12875. https://doi.org/10.1111/jeu.12875.
68. Tikhonenkov, D.V., Mikhailov, K.V., Hehenberger, E., Karpov, S.A., Prokina, K.I., Esaulov, A.S., Belyakova, O.I., Mazei, Y.A., Mylnikov, A.P., Aleoshin, V.V., and Keeling, P.J. (2020). New lineage of microbial predators adds complexity to reconstructing the evolutionary origin of animals. Curr. Biol. *30*, 4500–4509.e5. https://doi.org/10.1016/j.cub.2020.08.061.
69. Richards, C.S. (1975). Genetic factors in susceptibility of *Biomphalaria glabrata* for different strains of *Schistosoma mansoni*. Parasitology *70*, 231–241. https://doi.org/10.1017/s0031182000049696.
70. Schindelin, J., Arganda-Carreras, I., Frise, E., Kaynig, V., Longair, M., Pietzsch, T., Preibisch, S., Rueden, C., Saalfeld, S., Schmid, B., et al. (2012). Fiji: an open-source platform for biological-image analysis. Nat. Methods *9*, 676–682. https://doi.org/10.1038/nmeth.2019.
71. Sereno, F.L.a.M. (2023). Fixing *Biomphalaria glabrata* Snails for Dissection (BRI).
72. Chernin, E. (1963). Observations on hearts explanted in vitro from the snail *Australorbis glabratus*. J. Parasitol. *49*, 353–364.
73. Sminia, T., and Barendsen, L. (1980). A comparative morphological and enzyme histochemical study on blood cells of the freshwater snails *Lymnaea stagnalis, Biomphalaria glabrata*, and *Bulinus truncatus*. J. Morphol. *165*, 31–39. https://doi.org/10.1002/jmor.1051650104.
74. Gilbertson, C.R., and Wyatt, J.D. (2016). Evaluation of euthanasia techniques for an invertebrate species, land snails (*Succinea putris*). J. Am. Assoc. Lab. Anim. Sci. *55*, 577–581.
75. Cham, B.E., and Knowles, B.R. (1976). A solvent system for delipidation of plasma or serum without protein precipitation. J. Lipid Res. *17*, 176–181. https://doi.org/10.1016/S0022-2275(20)37003-6.

STAR★METHODS

KEY RESOURCES TABLE

REAGENT or RESOURCE	SOURCE	IDENTIFIER
Biological samples		
Biomphalaria glabrata hemolymph (snail serum)	This paper	N/A
Biomphalaria glabrata hemolymph extracted lipids (snail serum lipids)	This paper	N/A
Chemicals, peptides, and recombinant proteins		
Dynole 34-2 Endocytosis Inhibitor	Neta Scientific	CAYM-34073-1
18:1/18:1/0:0 glyceryl dioleate (DG)	Sigma	D3627
glyceryl trioleate (TG)	Sigma	T7140
dioleoyl phosphatidylcholine (DOPC)	Avanti Polar Lipids	850375P
18:1/24:0 ceramide (Cer)	Avanti Polar Lipids	860524P
palmitoyl lysophosphatidylcholine (LPC)	Avanti Polar Lipids	855675C
Deposited data		
Lipidomics analysis of snail serum samples	This paper	MSV000094067
Proteomics analysis of snail serum samples	This paper	MSV000094051
Experimental models: cell lines		
Capsaspora owczarzaki strain ATCC®30864	Iñaki Ruiz-Trillo (Suga et al.[22])	ATCC®30864
Capsaspora owczarzaki strain ATCC®50973	ATCC	ATCC®50973
Capsaspora owczarzaki strain ATCC®50974	ATCC	ATCC®50974
Capsaspora owczarzaki strain ATCC®30864+TdTomato	This paper	ATCC®30864+TdTomato
Experimental models: organisms/strains		
Biomphalaria glabrata strain NMRI	Biomedical Research Institute (Rockville, MD) (BRI) Schistosomiasis Resource Center	*B. glabrata* NMRI
Biomphalaria glabrata strain M-line	Sam Loker Lab, University of New Mexico, Biomedical Research Institute (Rockville, MD) (BRI) Schistosomiasis Resource Center (Richards et al.[69])	*B. glabrata* M-line
Schistosoma mansoni PR1 (Puerto Rican Strain 1) cercariae	Sam Loker Lab, University of New Mexico, Biomedical Research Institute (Rockville, MD) (BRI) Schistosomiasis Resource Center	*S. mansoni* PR1
Oligonucleotides		
PCR outer primers Capsa_28AS ATCCTTGTTAGTTTCTTTTC	Integrated DNA Technologies	Capsa_28AS
PCR outer primers Capsa_7S GGACTTTTACTGTGAAAAAA	Integrated DNA Technologies	Capsa_7S
PCR inner primers Capsa_7AS CTTGTAGGGGTGAGTTTAGG	Integrated DNA Technologies	Capsa_7AS
PCR inner primers Capsa_5S GGAGAAAGAAAAAAAAAGGA	Integrated DNA Technologies	Capsa_5S

(*Continued on next page*)

Continued

REAGENT or RESOURCE	SOURCE	IDENTIFIER
Recombinant DNA		
TdTomato expression construct for *Capsaspora owczarzaki*	This paper	Addgene (#213505) pJG01
Software and algorithms		
Fiji Imaging Software version 2.1.0/1.53c	Schindelin et al.[70]	https://imagej.net/software/fiji/
Bitplane Imaris Imaging Software version 10.0.1	Oxford Instruments Bitplane Imaris RRID:SCR_007370 http://www.bitplane.com/imaris/imaris	Imaris (RRID:SCR_007370) http://www.bitplane.com/imaris/imaris

EXPERIMENTAL MODEL AND STUDY PARTICIPANT DETAILS

Capsaspora *owczarzaki* cell cultures (strain ATCC30864)

Capsaspora owczarzaki cell cultures (strain ATCC®30864) were grown axenically in 25 cm^2 culture flasks with 6 mL ATCC media 1034 (modified PYNFH medium) containing 10% (v/v) heat-inactivated Fetal Bovine Serum (FBS, Corning 35-011-CV), hereafter *growth media*, in a 23°C incubator. Adherent stage cells (filopodiated amebae) at the exponential growth phase were obtained by passaging ~100–150 μL of adherent cells at ~90% confluence in 6 mL of growth media and grown for 24–48 h at 23°C until ~100% confluent.

M-line Capsaspora *owczarzaki* cell cultures (strain ATCC50973)

M-line *Capsaspora owczarzaki* cell cultures (strain ATCC®50973) were grown axenically in 25 cm^2 culture flasks with 6 mL *growth media*, in a 23°C incubator. Cells were maintained by passaging ~1 mL of adherent cells at ~1x10^6 cells/mL in 5 mL of growth media and grown for 1 week at 23°C until ~100% confluent.

Salvador *Capsaspora owczarzaki* cell cultures (strain ATCC50974)

Salvador *Capsaspora owczarzaki* cell cultures (strain ATCC®50974) were grown axenically in 25 cm^2 culture flasks with 6 mL *growth media*, in a 23°C incubator. Cells were maintained by passaging ~3 mL of adherent cells at ~2.8x10^6 cells/mL in 3 mL of growth media and grown for 1 week at 23°C until ~100% confluent.

Biomphalaria glabrata NMRI snails

Biomphalaria glabrata NMRI snails were obtained from the Biomedical Research Institute (Rockville, MD) (BRI) Schistosomiasis Resource Center. Snails were kept in tanks with about 5 L of artificial pond water (BRI protocol: 0.46 μM $FeCl_3$, 220 μM $CaCl_2$, 100 μM $MgSO_4$, 310 μM KH_2PO_4, 14 μM $(NH_4)_2SO_4$ in water adjusted to pH 7.2 with NaOH) with no more than 50 snails per tank until experiments were conducted. Snails were fed romaine lettuce once per week or earlier if they ran out unless otherwise stated. Pond water was changed once per week, or sooner if water was cloudy, by transferring all snails into a new tank with fresh artificial pond water. Hemolymph was collected from snails that were 12–17 mm in diameter. *B. glabrata* are hermaphrodites.

Biomphalaria *glabrata* M-line snails

Biomphalaria glabrata outbred M-line snails were maintained in plastic 20 L tanks filled with 15 L of artificial pond water with no more than 30 snails per tank. Snails were fed red leaf lettuce and 2 Wardly shrimp pellets 2 times a week. The water was changed once per month. Snails were maintained between 25°C and 27°C on a 12h:12h light-dark cycle. Hemolymph was collected from snails that were 7–10 mm in diameter. *B. glabrata* are hermaphrodites.

METHOD DETAILS

General microscopy methods

All aggregation assays were performed at room temperature. Brightfield imaging was performed using the following instruments: Leica DMi1 inverted microscope with an MC120 HD camera, Leica DMIL inverted microscope with Flexacam C3 camera, an Olympus OSR spinning disk confocal microscope with a Hammamatsu Flash 4 V2 camera, and an Incucyte S3 Live-Cell Analysis System. Depending on well size and microscope used, each well was imaged at up to 3 distinct locations using 5X or 10X magnification. Average aggregate areas were typically measured by batch processing with a standard macro script in Fiji Imaging Software[27,70] (see *Image analysis* below).

Generating a *Capsaspora* line stably expressing tdTomato

(related to Figures 1C–1E and S4–S6) A tdTomato expression plasmid was generated from plasmid pJP72.[26] The tdTomato gene was synthesized by GenScript with codons optimized for *Capsaspora*. The gene was cloned into pJP72, replacing the mScarlet protein-coding region. The resulting plasmid (pJG01) is available from Addgene (#213505), and its sequence is deposited there (www.addgene.org). *Capsaspora* cells (strain ATCC30864) were transfected following the protocol by Phillips et al. (2022).[26] Briefly, on the first day, $3*10^5$ cells in exponential growth phase were seeded in 800 μL onto sterile 12 mm circular glass coverslips in a well of a 24-well plate and allowed to settle overnight. On the second day, the growth medium was removed and replaced with transfection medium (Scheider's Drosophila Medium with 10% (v/v) FBS, supplemented with 25 μg/mL ampicillin) and allowed to incubate for 10 min. Two samples each were treated with Opti-MEM with 2 μg of transfection DNA (either pJG01, or negative control without DNA) along with TransIT-X2 transfection reagent (Mirus Bio) premixed and allowed to incubate 5 min at room temperature. Cells were treated with 70 μL of transfection mix and incubated at 23°C for 24 h. On the third day, the transfection medium was removed and replaced with standard growth medium, and cells were allowed to recover for 24 h. On the fourth day, growth medium was removed and replaced with medium supplemented with selective drug (Geneticin at 320 μg/mL). Transfected cells were grown in selective medium for two weeks changing media with fresh selective media every 3 days. Cells in the negative control wells were dead after one week of drug selection. Red fluorescence from tdTomato-positive cells was screened on an Olympus spinning disk confocal microscope using a 561 nm laser, which confirmed >99% of cells expressed tdTomato. After two weeks, the culture of cells was diluted to extinction to afford multiple single clones, which all maintained fluorescence in the absence of antibiotic selection and continued to aggregate similarly to the parent. *In vitro* aggregation for the clone used in this study is reported in Figure S10.

Injection of fluorescent *Capsaspora* into snail tissue

(related to Figures 1C–1E, S1C, and S1D) Snails were prepared and mounted on microscope slides according to the BRI protocol.[71] Briefly, snails measuring between 6 and 20 mm were placed in hot artificial pond water (70°C) for 50 s, then immediately submerged into a cold water bath for 60 s. Snails were removed from their shell by gently pulling on the foot with forceps and placed on microscope slides for injection. Snails were injected using glass capillary needles (World Precision Instruments, 1B100F-6) pulled to an opening size of approximately 100 μm with a Model P-87 Sutter Instrument Micropipette Puller. Two days before the experiment, a 100% confluent flask of *Capsaspora* cells stably expressing tdTomato were "fed" by replacing the selective growth media with fresh selective growth media. The day before the experiment, the *Capsaspora* cells were washed and resuspended in FBS-free media containing no antibiotics and allowed to starve overnight. On the day of the experiment, cells were washed and then resuspended with Chernin's balanced salt solution (CBSS+)[72] before injection. Snails were injected with 20 μL of *Capsaspora* cells suspended in balanced salt solution ($4*10^7$ cells/mL) into their mantle cavity or pericardium. After injection, needles were left in the tissue for several minutes to allow the hemolymph to clot and prevent *Capsaspora* from bleeding back out. To determine if aggregation was calcium dependent, the calcium chelator EGTA was pre-mixed with cells to a final concentration of 250 mM before injecting 20 μL into snails. As a negative control, cells were injected through the needle directly onto a microscope slide with no snail. Also, snails that were never injected were imaged (no red fluorescent cells of the correct size were observed). Red fluorescence was imaged using an Olympus spinning disk confocal microscope with a 547 nm excitation laser. Brightfield and green fluorescence (488 nm) images were taken as well to see surrounding snail tissue structure.

General method for harvesting snail serum

Serum was harvested from snails measuring between 7 and 17 mm. Snails were removed from their growth tanks, rinsed with autoclaved water, and dried with paper towels or KimWipes. Serum was harvested by the headfoot retraction method.[73] Briefly, using 200 μL micropipettes or 1 mL glass pipettes, the tip was tapped gently onto the snail headfoot, causing it to retract and hemolymph to pour out from the hemal pore. As the foot retracted, serum was collected into the pipette tip and transferred to microcentrifuge tubes. After harvesting all possible serum, snails were placed in stage 1 of a 2-stage euthanasia solution[74] (95% (v/v) water +5% (v/v) ethanol) for 10 min, and then transferred to stage 2 (95% (v/v) ethanol +5% (v/v) water) for 5 min. Tubes containing snail serum were centrifuged at 14,000xg for 15 min to move any mucus collected to the top of the tube. Bright red, transparent serum was collected from the bottom of the tube and diluted 1:1 in Chernin's balanced salt solution (CBSS+)[72] before sterile filtering through at 0.22 μm filter. Sterile serum was stored at 4°C until use.

Aggregation assay on ultra-low attachment plates

(related to Figures 1F–1K, 2A, 2E, 2I, 2J, 2M, 3A–3C, 4A, 4B, S2–S4, S6, and S10) These assays were always performed with strain ATCC30864. Two days before the assay, 100% confluent adherent cells growing in 25 cm^2 culture flasks were given fresh growth media (termed the "feed step"). One day before the assay, cells were washed and resuspended in FBS-free assay media and allowed to sit overnight (termed the "starve step"). After starvation, the day of the assay, $8*10^5$ cells were seeded in 180 μL of FBS-free media per well in a 96-well ultra-low attachment microplate (#CLS3474, Corning) and allowed to settle for 2 h. Putative aggregation inducers were added such that the total volume in a well was 200 μL. Typically, aggregates were assessed by microscopy after 90 min.

Image analysis for aggregation assays

(related to Figures 1F–1K, 2A, 2E, 2I, 2M, 3A–3C, 4A, 4B, and S2) Average aggregate areas were typically measured by batch processing with a standard macro script in Fiji Imaging Software version 2.1.0/1.53c.[27,70] Briefly, the macro steps included: set the scale of the image appropriate

for the microscope conditions, convert the image to binary, analyze particles (size 0-infinity), export results to clipboard. A copy of the FIJI macro is available upon request.

In vitro analysis of snail serum aggregation

(related to Figure 1F) The standard aggregation assay on ultra-low attachment plates (using *Capsaspora* strain ATCC30864) was used to assess activity of 100% (v/v) snail serum compared to 5% (v/v) FBS or 5% (v/v) phosphate-buffered saline (PBS, Gibco 14190144, 138 mM NaCl, 8.06 mM Na_2HPO_4, 2.67 mM KCl, 1.47 mM KH_2PO_4) in assay media. After seeding cells, FBS-free assay media was removed by aspiration and replaced with 100% 1X snail serum harvested by the headfoot retraction method or media containing 5% (v/v) FBS or 5% (v/v) PBS. Images of triplicate assay wells were taken every 30 min and example images are shown from T-90 min.

Snail serum fractionation

(related to Figures 1G and 1H) Snail serum was fractionated using Amicon Ultra 30 kDa cutoff filters (Sigma, # UFC5030) according to the manufacturer's directions. Briefly, the filter was first washed with 500 μL of PBS by centrifugation at 14,000xg for 15 min. Then 500 μL of harvested serum was added to the cutoff filter and centrifuged at 14,000xg for 15 min. The <30 kDa fraction was collected while the >30 kDa fraction was washed three more times with PBS. The standard aggregation assay on ultra-low attachment plates was used to assess activity of 50% (v/v) whole unfractionated snail serum, 50% (v/v) > 30 kDa snail serum, and 50% (v/v) < 30 kDa snail serum, compared to 5% (v/v) FBS or 5% (v/v) PBS in media. A dilution series of >30 kDa snail serum was also tested using this method. Images of triplicate assay wells were taken every 30 min and analysis was performed on images from T-90 min. Average aggregate areas were measured by batch processing with the FIJI macro script reported above.

Aggregation assay for M-line and salvador strains

(related to Figures 1L and S5) Due to the inability of M-line and Salvador strains to settle at high densities onto the sufaces of the culture vessels, an alternative aggregation assay using orbital agitation was employed. *Capsaspora* cells ($8*10^6$ cells/mL) were washed and resuspended in growth media *without FBS,* hereafter referred to as *assay media,* and seeded into a 24-well plate ($4*10^6$ cells per well). Aggregation inducers were added: 10% (v/v) FBS, 50% (v/v) > 30 kDa snail serum, or 10% (v/v) PBS as a negative control), and the plate was agitated at 50 rpm overnight (Celltron Bench-Top Shaker, INFORS-HT). Aggregates were assessed by microscopy after ~11.5h. Average aggregate area was measured with the FIJI macro script described above.

Morphological analysis of tdTomato-expressing *Capsaspora* cells

(related to Figures S3A, S3B, S3E, S4, and S6) The standard aggregation assay was run using tdTomato expressing *Capsaspora* cells (derivatives of strain ATCC30864). Aggregates were induced with either 5% (v/v) FBS or 50% (v/v) > 30 kDa snail serum, or a dilution series of pure DOPC vesicles (preparation described below) and 3D z-stacks were taken of each replicate well monitored every 4 h for 48 h using a Cytation C10 imager (Agilent) with confocal 546 nm excitation laser, laser autofocus, and a 20x objective. Three-dimensional z-stacks from the time point after 4 h of induction were analyzed using the Imaris batch processing macro described below.

Morphological analysis of propidium iodide-stained aggregates

(related to Figures S3C, S3D, S3F, S4, and S6) *Capsaspora* aggregates (strain ATCC30864) were prepared following the standard aggregation assay protocol in ultra-low attachment plates (under "General aggregation assay methods" near the start of Methods section). Aggregates were induced with either 5% (v/v) FBS or 50% (v/v) > 30 kDa snail serum, or a dilution series of pure DOPC vesicles (preparation described below). About 14 h after induction of aggregates, cells in assay plates were fixed with 4% (v/v) formaldehyde for 30 min. Fixed aggregates were washed three times with PBS and then stained with 0.02 mg/mL propidium iodide (PI) for 1 h. Stained aggregates were washed three times with PBS to remove excess PI before imaging. Cells were imaged using an Olympus spinning disk confocal microscope with 546 nm excitation laser. Three-dimensional z-stacks of aggregates were analyzed using the Imaris batch processing macro described below.

Image analysis of 3D confocal experiments

(related to Figures S3–S6) Three-dimensional z-stacks of aggregates were analyzed by batch processing with Bitplane Imaris Imaging Software version 10.0.1. Briefly, the batch protocol was as follows: create Surfaces, surface grain size = 3 μm, manual threshold 82.114, add Spots, estimate diameter 3.51 μm, background subtraction, "Quality" above automatic threshold, classify spots based on distance to surfaces, threshold 2.91 μm (inside surface), export statistics: surface sphericity, surface intensity inside, number and classification of spots, surface area, surface volume, surface bounding box oriented dimensions. A copy of the Imaris batch protocol is available upon request.

Aggregation dynamics over time

(related to Figures 1I–1K, S2, and 2M; Videos S1, and S2) The standard aggregation assay on ultra-low attachment plates (using *Capsaspora* strain ATCC30864) was used to assess activity of 5% (v/v) FBS, 50% (v/v) > 30 kDa snail serum, or 63 μg/mL DOPC vesicles over time. The corresponding volume of PBS was used as a negative control. Plates were imaged every 20 min using the 4X objective on an Incucyte S3 Live-Cell Analysis System. Aggregates were induced 1 h after initiating Incucyte reads, and plates were kept at 23°C by the system while incubating

between images. Resulting image stacks from triplicate wells were first converted into binary and average aggregate area, as well as average aggregate circularity (calculated as the ratio of *x* and *y* bounding box dimensions), was calculated by batch processing with a macro script in FIJI adapted to analyze time stacks. Briefly, the macro is set to: set scale, make binary, Gaussian blur (sigma = 4), run "analyze particles" size 3–100000, count, and summarize results. The summary results that were plotted were: average particle area, and circularity (calculated by the ratio of 2D bounding box dimensions). A copy of the FIJI stacks macro is available upon request. Representative binary images from selected time-points are shown.

Extraction of lipids from snail serum

(related to Figures 2A–2D) Snail serum was harvested by the headfoot retraction method.[73] Lipids were extracted from serum following a protocol from Cham and Knowles (1976).[75] Briefly, 0.1 mg of EDTA was added to 1 mL of serum in a 4-dram vial. Then, 2.5 mL of premixed 25:75 (v/v) butanol to diisopropyl ether (DIPE) was added. The solution was rocked gently at a speed of 50 on a Fisherbrand Digital Platform Rocker for 3 h. After rocking, the vials were allowed to sit for 15 min until the layers separated. The organic layer was carefully removed from the aqueous layer. Note that no proteins in the aqueous layer precipitated. The organic layer was completely evaporated using a Savant SpeedVac SPD2030 at 45°C under 5.1 millitorr of vacuum pressure for 2 h. Lipids were extracted separately from the sera of three batches of snails (10 NMRI snails per batch, ~100 μL/snail) and stored at −20°C until use.

Preparing lipid vesicles from lipid extracts and pure lipids

(related to Figures 2 and S3–S6) Lipids extracted from snail serum samples or commercially obtained (pure synthetic lipids) were redissolved in chloroform in glass vials and transferred to a 1.7 mL microcentrifuge tube. The chloroform was evaporated using a gentle stream of nitrogen and the resulting lipid film was then resuspended in 1 mL each of PBS. The tubes were vortexed for 30 s before sonication. Lipid solutions were sonicated on ice with a 50% duty cycle at medium setting for 10 min using a single probe attached to a Branson Sonifier Cell-Disruptor 185. During sonication, tubes were kept on ice and tube bottoms were set about 3 mm from the sonicator tip. Lipid solutions went from slightly cloudy to clear after sonication. Sonicated lipids were stored at 4°C for no more than 2 days before use.

In the case of crude snail serum lipids (Figures 2A–2D), all the lipids were extracted from 1 mL of snail serum (from 10 snails, each ~12–17 mm, ~100 μL/snail), resulting in ~0.3 mg of dried crude lipids. After extracting and drying, crude lipids were reconstituted in 1 mL of PBS and sonicated. Therefore, the extracted lipids were present at their natural serum concentration. Crude solubilized lipids were concentrated 10X using a >30 kDa cutoff filter in the same way as snail serum before addition into assay wells. The resuspended lipids exhibited similar potency (v/v) as snail serum.

In the case of the simple lipid mix (Figures 2E–2H), initial amounts of lipids were chosen based on the ratio of $[M + H]^+$ intensity values calculated in the snail serum lipidomics analysis. Commercially available lipids in each of the five most prevalent classes were chosen to make the mix. The simple mix contained 100 μg of glyceryl dioleate (DG), 150 μg of glyceryl trioleate (TG), 200 μg of DOPC (PC), 10 μg of 18:1/24:0 ceramide (Cer), and 10 μg of palmitoyl lysophosphatidylcholine (LPC) for a total of 470 μg of lipid in 1 mL of PBS. Later, mass spectrometry of formed vesicles revealed a true ratio of about ~42% DG, ~15% TG, ~40% PC, ~1.5% Cer, and ~1.5% LPC incorporated into the simple lipid vesicles. As above, the solubilized simple lipid mix was concentrated 10X using a >30 kDa cutoff filter before addition into assay wells and concentrations were reported in μg/mL based on final lipid mass/volume of the assay well.

In the case of pure DOPC vesicles (Figures 2I–2L and S6), 220 μg of DOPC was used for each 1 mL of vesicles prepared in PBS. As above, the DOPC vesicles were concentrated 10X using a >30 kDa cutoff filter before addition into assay wells and concentration was reported in μg/mL based on mass of DOPC/volume of the assay well.

Testing lipid vesicles for aggregation

(related to Figures 2A–2E, 2I, and 2J) Sonicated lipids were concentrated 10X using an Amicon Ultra 30 kDa cutoff filter and diluted with PBS to the desired concentration before testing. The standard aggregation assay on ultra-low attachment plates (using *Capsaspora* strain ATCC30864) was used to test for aggregation induction. Aggregates were induced using the desired lipid concentration (calculated in μg/mL of lipid) and 5% (v/v) of PBS was used as a negative control. Aggregates in triplicate wells were imaged every 30 min and analysis was performed on images from T-90 min. Average aggregate areas were measured using a macro in FIJI as described above.

Transmission electron microscope (TEM) imaging of lipid vesicles

(related to Figures 2B–2F and 2K) Before preparation of samples, Formvar/Carbon film 300 mesh Nickel Grids (Electron Microscopy Sciences FCF300-Ni-25) were ionized using a Pelco easiGlow Discharge System at 0.3 mbar and 15 mAmps for 2 min. 10 μL of prepared lipid samples were added to the ionized grids and allowed to sit for 5 min. Excess sample was removed from the grids by gently touching Whatman filter paper (Sigma, WHA1001329) to the edge. Immediately after removing samples (before grid dries) 10 μL of 2% (v/v) Uranyl Acetate pre-diluted in water was added to grids and allowed to sit for 10 s. Then the stain was removed with the edge of Whatman filter paper. Grids were allowed to dry completely before imaging (about 10 min). Prepared grids were imaged using a JEOL-JEM 1010 transmission electron microscope (TEM) with an 80 kV operating voltage, equipped with a 1k x 1k Gatan CCD camera (MegaScan model 794) using a tungsten filament as its electron source.

Dynamic light scattering of lipid vesicles

(related to Figures 2C–2G and 2L) 400 μL of prepared lipid vesicles suspended in PBS at room temperature were transferred to a BRAND UV micro disposable cuvette (BR759200-100EA) and placed in a Malvern Panalytical Zetasizer Nano ZS DLS. Size measurements were recorded in a range of 0.3 nm–3 mm as raw intensity and then normalized based on particle size using the Malvern software to give the final distribution of particle sizes in each sample. The "number" distribution was plotted and Z-averages (nm) were reported. Triplicate measurements were recorded for each sample.

Mass spectrometry of lipid samples

(related to Figures 2D–2H, 3D–3F, 4C–4E, and S7; Table S1) For most lipidomics analysis, fully dried lipid samples were shipped to the Beth Israel Deaconess Medical Center (BIDMC) Metabolomics Core. The LC-MS/MS based non-polar lipidomics profiling work was conducted by Dr. John Asara at the BIDMC Mass Spectrometry Core in Boston, MA USA. For calculation of the amount of DOPC in snail serum samples, 1 mL of snail serum was spiked with a known volume of SPLASH Lipidomix II mass spectrometry standard (Avanti Polar Lipids, #330709) and then extracted according to the method described above. Dried lipid samples were resuspended in 2:1 (v/v) isopropanol/methanol. High-resolution electrospray ionization (HR-ESI) mass spectra with collision-induced dissociation (CID) MS/MS were obtained using an Agilent LC-q-TOF mass spectrometer 6530 equipped with an Agilent 1290 uHPLC system. Metabolites were separated using a Luna 5 μm C5 100 Å LC column (Phenomenex 00D-4043-E0). Mobile phase A was 95% (v/v) Water, 5% (v/v) Methanol, 0.1% (v/v) Formic Acid, and 5 mM Ammonium Formate. Mobile phase B was 60% (v/v) Isopropanol, 35% (v/v) Methanol, 5% (v/v) Water, 0.1% (v/v) Formic Acid, and 5 mM Ammonium Formate. After initially holding 0% phase B for 5 min at 0.1 mL/min, a linear gradient from 20% phase B to 100% phase B was applied over 40 min with a flow of 0.4 mL/min before holding at 100% phase B for another 5 min with a flow of 0.5 mL/min. Data-dependent acquisition was employed to fragment the top masses in each scan. CID was applied using a linear formula that applied a higher voltage for larger molecules (CID voltage = 10 + 0.02 m/z)for metabolite profiling and identification. Mass traces collected in positive mode were analyzed in MassLynx software v4.1 and calculated concentrations were normalized to the known concentration of the internal SPLASH standard.

Infection of M-line snails with PR1 schistosomes

(related to Figures 3 and 4) Two mice were exposed to 150 PR1 (Puerto Rican Strain 1) cercariae from snails originally exposed to BRI-derived miracidia, the resulting miracidia from those two mice were used to expose 120 5–6 mm *B. glabrata* M-line snails to 10 PR1 miracidia. All miracidia displayed positive phototaxis, normal shape, and swimming behavior. Snails were exposed for 2 h in 12-well cell culture plates and then placed into 4 different 20 L tanks. 60 5–6 mm *B. glabrata* M-line snails were sham-exposed (no parasites) in 12-well cell culture plates for 2 h and placed into 3 different 20 L tanks as control snails. Experimental snails were fed 3 times a week red leaf lettuce and 2 Wardly shrimp pellets. Snails were maintained between 25°C and 27°C on a 12h:12h light-dark cycle. After 28, 32 and 38 days post-exposure, snails were checked to determine if cercariae were being released (shedding). Snails were placed in 12-well cell culture plates for 2 h between 10:00 a.m. to 12:00 p.m. under light. At 38 days post-exposure, 79 *B glabrata* M-line snails were shedding cercariae (group 1: $n = 20$, group 2: $n = 20$, group 3: $n = 20$, group 4: $n = 19$). Sham-exposed control snails were in 3 different groups (group 1: $n = 20$, group 2: $n = 20$, group 3: $n = 11$). At this point, snails were 7–10 mm, and serum was collected and pooled within each group (4 groups for infected, 3 groups for sham-exposed control).

Measuring aggregation induced by naive and infected M-line snail serum and naive NMRI snail serum

(related to Figures 3A–3C, 4A, and 4B) The standard aggregation assay using ultra-low attachment plates (using *Capsaspora* strain ATCC30864) was used to determine aggregation potency of snail serum samples. Serum collected from three separate batches of naive or infected snails were each concentrated to 5X using an Amicon Ultra 30 kDa cutoff filter. Aggregation was induced by a dilution series of each of the >30 kDa snail serum samples. Assay wells were imaged every 30 min and representative images from T90 min are shown. Average aggregate area was calculated by batch processing with the standard macro script in FIJI as described above.

Proteomics analysis of snail serum samples

(related to Figures 4F and S8; Table S2) Serum harvested from three separate batches of naive NMRI (10 snails per batch), naive M-line (batches of $n = 20$, $n = 20$, and $n = 11$ snails), and infected M-line snails (batches of $n = 20$, $n = 20$, and $n = 20$ snails) via the headfoot retraction method were submitted for untargeted proteomics analysis by the Laboratory for Biological Mass Spectrometry at Indiana University.

QUANTIFICATION AND STATISTICAL ANALYSIS

Statistical details of the experiments, where applicable, can be found in figure legends. In all cases, an asterisk indicates $p < 0.05$ by a Student's t test.